nature neuroscience

Article

https://doi.org/10.1038/s41593-023-01446-w

Rapid compensatory plasticity revealed by dynamic correlated activity in monkeys in vivo

Received: 10 March 2022

Accepted: 1 September 2023

Published online: 12 October 2023

Check for updates

Ariana R. Andrei[1] ✉, Alan E. Akil[2], Natasha Kharas[1], Robert Rosenbaum[3], Krešimir Josić[2] & Valentin Dragoi[1,4] ✉

To produce adaptive behavior, neural networks must balance between plasticity and stability. Computational work has demonstrated that network stability requires plasticity mechanisms to be counterbalanced by rapid compensatory processes. However, such processes have yet to be experimentally observed. Here we demonstrate that repeated optogenetic activation of excitatory neurons in monkey visual cortex (area V1) induces a population-wide dynamic reduction in the strength of neuronal interactions over the timescale of minutes during the awake state, but not during rest. This new form of rapid plasticity was observed only in the correlation structure, with firing rates remaining stable across trials. A computational network model operating in the balanced regime confirmed experimental findings and revealed that inhibitory plasticity is responsible for the decrease in correlated activity in response to repeated light stimulation. These results provide the first experimental evidence for rapid homeostatic plasticity that primarily operates during wakefulness, which stabilizes neuronal interactions during strong network co-activation.

The brain is continuously bombarded with sensory information during active wakefulness. Repeated exposure to external stimuli during environment exploration has been hypothesized to induce changes in cortical networks via associative (or 'Hebbian') plasticity, which increases the strength of synaptic connections based on the cofiring of presynaptic and postsynaptic neurons. However, an excessive increase in synaptic strengths may limit the ability of cortical neurons to respond to their inputs[1]. To prevent this unwanted situation, computational studies have proposed various forms of homeostatic plasticity to restore neural activity to baseline levels after changes in synaptic input, and hence provide the necessary stabilization of network function[2]. Nonetheless, while experimental studies have shown that associative plasticity can be rapidly induced within seconds to minutes, homeostatic mechanisms were shown to operate on the order of days[3]. This timescale difference is problematic[4] as numerous studies have indicated that associative plasticity needs to be rapidly counterbalanced to prevent runaway network dynamics[2]. As a solution to this problem, computational studies have long posited the existence of rapid compensatory processes, possibly mediated by inhibitory plasticity, but experimental evidence for such rapid mechanisms has been elusive[5].

A possible reason for the lack of evidence for rapid, compensatory processes is that in vivo homeostatic processes have been primarily studied by examining neuronal firing rates in response to sensory deprivation whereby responses return to baseline only after 24–48 h (refs. 6,7). However, it is conceivable that rapid compensatory processes could initially alter neuronal connectivity without dramatically altering individual neuron firing rates. For instance, heterosynaptic plasticity[8] leads to the weakening of synapses located adjacent to

[1]Department of Neurobiology and Anatomy, University of Texas, Houston, TX, USA. [2]Departments of Mathematics, Biology and Biochemistry, University of Houston, Houston, TX, USA. [3]Department of Applied and Computational Mathematics and Statistics, University of Notre Dame, Notre Dame, IN, USA. [4]Department of Electrical and Computer Engineering, Rice University, Houston, TX, USA. ✉e-mail: ariana.r.andrei@uth.tmc.edu; valentin.dragoi@uth.tmc.edu

potentiated synapses over the course of hours. Thus, if some proportion of synapses are potentiated, some depressed and others are left unchanged, the net effect on neurons' firing rates could be minimal, while local network connectivity structure could be markedly altered.

Measuring dynamic changes to cortical network connectivity in vivo is challenging, although they can be identified by combining measures of shared variability with computational models. Cortical pyramidal neurons can produce virtually identical spiking responses in vitro[9], while in vivo, responses to identical stimuli are much more irregular. In sensory cortical circuits, this neural variability is shaped by a combination of biophysical properties of neurons and interlaminar and local intralaminar synaptic connectivity[10]. Spike-count correlations measure the similarity of this variability between pairs of cortical neurons and are therefore shaped by both circuit structure and cellular properties, and frequently reflect shared, common synaptic input[10–13]—the more inputs a pair of cells share, the higher their spike-count correlations. For example, neurons located in specific cortical layers receiving a higher percentage of common inputs are typically characterized by higher spike count correlations[14]. Notably, spike-count correlations themselves have been shown to be altered during classic homeostatic plasticity that occurs on very long timescales (days) following sensory deprivation[15]. Further, it has been recently demonstrated that such long-timescale homeostatic regulation is mediated by selective changes to network-related dendritic spines (rather than sensory-related spines)[16], suggesting that homeostatic plasticity alters local cortical connectivity rather than thalamo-cortical projections.

Here we combine optogenetic stimulation, cortical recordings and computational modeling to examine whether rapid homeostatic regulation is reflected in changes to the local network correlation structure in response to repeated optogenetic stimulation of excitatory cells. We measured the dynamics of pairwise correlations between simultaneously recorded neurons in response to input perturbations in awake, task-engaged macaques (*Macaca mulatta*)[7,11,17]. We found that repeated optogenetic activation of excitatory V1 neurons induces a dynamic reduction in the strength of neuronal interactions during wakefulness, but not during rest, over a timescale of minutes. This new form of rapid plasticity was observed only in the correlation structure but not firing rates, which remained stable across trials. These results provide the first experimental evidence for rapid homeostatic plasticity that stabilizes network interactions during strong network co-activation primarily operating during wakefulness.

Results

Rapid compensatory plasticity

To probe rapid network plasticity in vivo, we stimulated a neural population using a protocol capable of inducing associative plasticity and monitored network connectivity dynamically. Specifically, we used optogenetic stimulation to repeatedly activate excitatory cells[18] in macaque primary visual cortex (V1; Fig. 1a). The stimulation protocol (35 Hz, 10 cycles and 10 ms pulse width) is similar to that used in previous studies to induce behaviorally relevant[19], lasting potentiation between excitatory neurons[20–22]. Here, however, we measured how each successive trial of light stimulation alters network connectivity by measuring network correlations. We expected associative plasticity to increase correlations by increasing the connection strength between pairs of excitatory neurons over time, while compensatory processes acting to mitigate associative plasticity would decrease correlations (Fig. 1a). Changes in firing rates can also rapidly change correlations, but on much shorter timescales[10].

To target glutamatergic neurons, we used a lentiviral vector carrying the genes for channelrhodopsin-2-green fluorescent protein (ChR2-GFP) under the control of the α-CaMKII promoter. This construct has been shown to express exclusively in glutamatergic (α-CaMKII expressing) neurons, with expression localized to the plasma membrane throughout the cell body and neuronal processes, and with no retrograde labeling[18]. Functionally, this opsin is able to reliably follow stimulation frequencies up to 50 Hz, although the probability of evoking a spike declines with long-lasting, high-frequency stimulation[18]. Following gene expression, we recorded the activity of cortical populations using multichannel laminar electrodes coupled to an optical fiber for light delivery (Fig. 1a; Methods). To maintain alertness and prevent unwanted fluctuations in cortical state during wakefulness, animals performed a stimulus detection task in which 50% of randomly interleaved trials included optogenetic stimulation (Fig. 1b,o, inset; Methods). We analyzed the changes in neuronal responses and pairwise correlations of light-responsive units (Methods) uncontaminated by stimulus presentation (0% contrast, 'c0') wherein animals maintained fixation on a gray screen to report the absence of a visual stimulus (sessions had a minimum of 118 trials).

As expected, optogenetic stimulation uniformly increased firing rates across trials during the 300-ms window aligned to laser onset (20 trials per block; Fig. 1c,d left, $n = 310$ units, Fig. 1e) relative to control (no light). Firing rates in the 300-ms interval following light stimulation were not[19,20] different from the control, nor did they vary from early to late trials (Fig. 1d, right). Next, we calculated spike count correlations dynamically (Fig. 1b) for all simultaneously recorded pairs of light-responsive neurons ($n = 2{,}413$ pairs) both within trials, in a 200-ms interval sliding every 50 ms (Fig. 1b, blue arrow), and across 20-trial blocks sliding each trial (Fig. 1b, magenta arrow). Surprisingly, correlations increased significantly during light stimulation on early blocks and then started to decrease in subsequent blocks[19,20] (Fig. 1f,g; $P = 4.7 \times 10^{-75}$, Kruskal–Wallis test, df = 39; post hoc $P = 3.5 \times 10^{-14}$, Wilcoxon signed rank test, first versus last trial blocks). This dynamic reversal was evident in individual sessions from each monkey (Fig. 1h). Further, the reversal of correlations across sequential trial blocks was evident regardless of whether correlations on laser trials were compared to control trials (Fig. 1g), or compared within laser trials across trial blocks (Fig. 1i, right). Eye position was not a confound as it remained stable across trials ($P = 0.331$, Kruskal–Wallis test, df = 3; Extended Data Fig. 1a–f) and laser conditions ($P = 0.974$, Kruskal–Wallis test, df = 7; Extended Data Fig. 1a–f). We did not find differences in the direction of microsaccades between laser and control conditions on early or late trial blocks (Extended Data Fig. 1g–i). The reduction of correlations in time was not due to a decrease in overall cell excitability, as evoked stimulus responses (oriented gratings, >5% contrast) did not differ between early and late trials (Extended Data Fig. 2; $P = 0.197$, Wilcoxon signed rank test control trials). Because correlations can be affected by the time window used for calculation[13], we also confirmed that using a much shorter (50 ms) window produced a similar reversal pattern (Extended Data Fig. 3a). Further, we also observed a similar reversal of correlations when we separately considered pairs of cells that were directly (0–2-ms latency) or indirectly (3–7-ms latency) activated by the light (Extended Data Fig. 3b). Lastly, we separately considered the pairs of cells that exhibited significant correlations on early control trials (compared to a null distribution of 1,000 shuffled correlations; Extended Data Fig. 3c) and found a similar decreasing trend across early to late laser trial blocks ($P = 8.92 \times 10^{-6}$, Wilcoxon rank-sum test, first versus last trial block), although correlations remained stable across control trials ($P = 0.184$, Wilcoxon rank-sum test, first versus last trial block). Thus, across repeated optogenetic stimulation trials, the strength of network interactions between light-responsive neurons progressively weakened, indicating the presence of an active compensatory process that decouples synchronously active neurons.

We next measured the timing of correlation reversal (Fig. 1g, red arrow). The trial block when the difference in correlations between laser and control switched from positive to negative (Fig. 1f–h, red arrows) occurred between 17.4 ± 1.16 and 25.4 ± 1.66 min from the start of each session (Extended Data Fig. 4a, trial blocks 8 and 20; mean ± s.e.m.) and comprised a total of 54.9 ± 1.23 to 79.1 ± 1.28 laser stimulation trials (Extended Data Fig. 4b, trial blocks 8 and 20, respectively).

https://doi.org/10.1038/s41593-023-01446-w

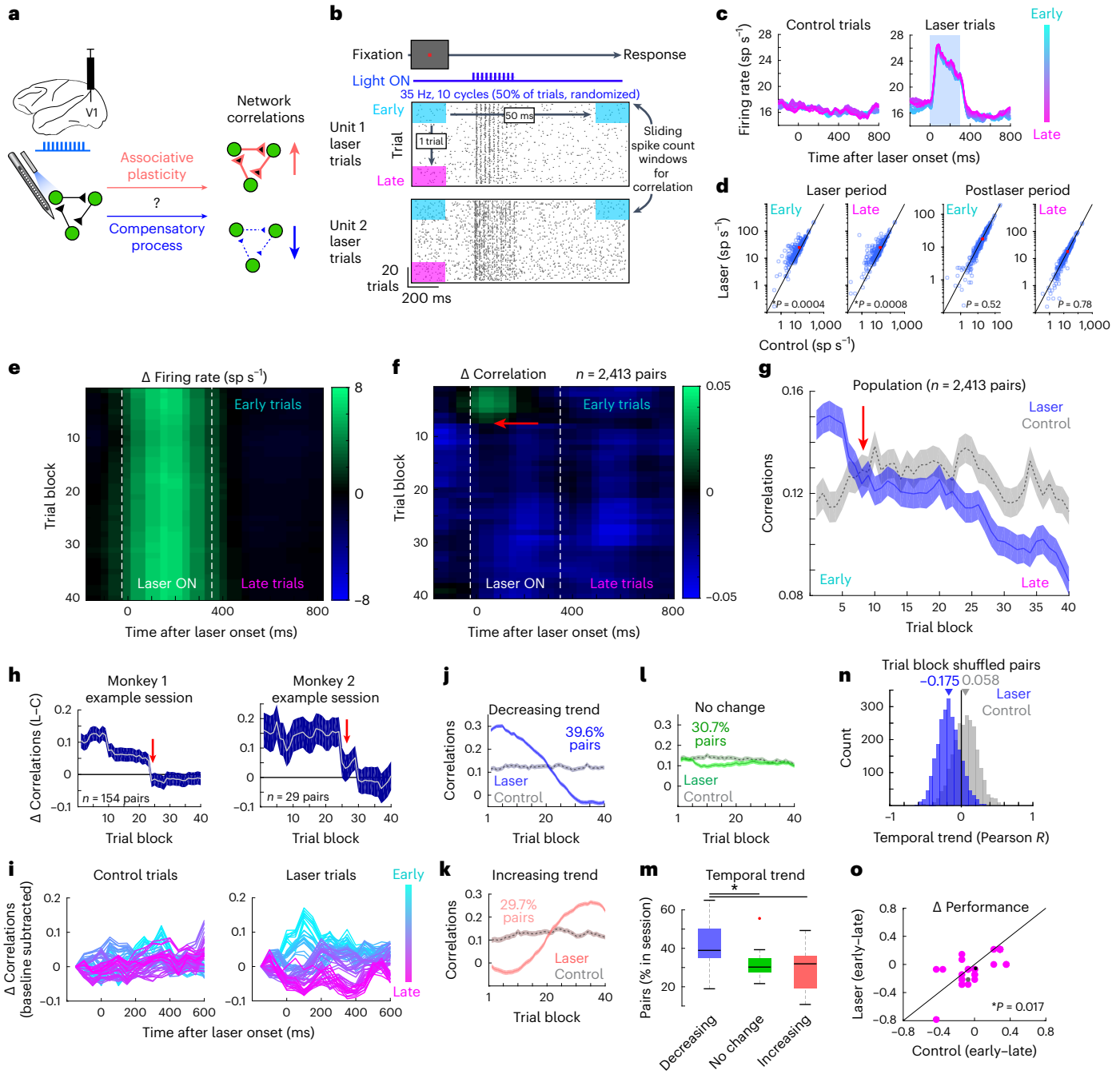

Fig. 1 | Strength of network connectivity progressively decreases with repeated optogenetic stimulation. a, Repeated stimulation of excitatory neurons (green circles) may increase or decrease network connectivity via associative potentiation (red) or compensatory (blue) processes. **b**, Top, trial structure; bottom, example laser trial rasters from one cell pair. Correlations were calculated using sliding windows of fixed size (colored rectangles). **c**, Population firing rates in laser (right) and control (left) trials across early to late blocks ($n = 310$ units). Blue shaded region denotes the time interval when light is presented. **d**, Optogenetically evoked changes in firing rate are not different between early and late trial blocks during laser (left) and postlaser periods (right) (Kruskal–Wallis tests, two-sided, left, $P = 3.15 \times 10^{-15}$, df = 3; right, $P = 0.785$, df = 3; P values show post hoc paired, two-tailed t-test results; $n = 349$ cells). Red dots show means. **e**, Firing rate difference between laser and control across all blocks of 20 trials for all pairs of laser-responsive neurons. **f**, Population mean correlation difference (laser minus control) across all blocks. Red arrow shows the trial block in which correlations reverse. **g**, Correlations in laser (blue) and control (gray) trials across early to late trial blocks. Traces and envelopes show mean ± s.e.m. **h**, Difference in correlations (laser minus control) for example sessions from each monkey. Line, mean; envelope, s.e.m. **i**, Example session showing baseline-subtracted correlation differences in control (left) and laser trials (right). Same session as in **h**, left. **j**, Mean correlation across trial blocks for all pairs with significant decreasing temporal trends across trial blocks. Traces show mean ± s.e.m., laser (blue) and control trials (gray). Percentage reflects pairs exhibiting pattern. **k**,**l**, Same conventions as **j**, but for increasing trend pairs (**k**), and remaining pairs (**l**). **m**, Distributions of temporal trend patterns within sessions. *$P = 0.0005$, Kruskal–Wallis test, post hoc Tukey test ($n = 2,413$ pairs). Box edges show 25th and 75th percentiles, central black line is the median and whiskers extend to the most extreme datapoints; outliers plotted in red. **n**, Temporal trends of shuffled pairs within each block for each session on laser (blue) and control (gray). Arrowheads show median of distributions (both significantly different from zero, $P < 0.001$ Wilcoxon signed rank test). **o**, Performance difference on laser versus control trials for early (first 14 trials) versus late (last 14 trials) blocks (*$P = 0.017$, Wilcoxon signed rank test, two-sided). Black star, median; gray circle, **h** (right) session.

The time course of the early increase in correlations (Fig. 1f, green area above red arrow) is similar to that of short-term potentiation ('STP'), which typically decays after ~20 min (refs. 20,21). However, STP cannot account for the continued decrease in correlations in late trial blocks.

Do all neurons co-activated by light become less coupled across trials? Examining the dynamics of individual pairs revealed that the greatest proportion of pairs showed a significant decrease in correlations across blocks (39.6% of pairs; Fig. 1j–m and Extended Data Fig. 5a–d), consistent with an underlying compensatory process (Pearson correlation values >0.3 or <−0.3 were considered significant, based on a sample size of 40 trials blocks and $\alpha = 0.05$). A minority of pairs (29.7%) showed the opposite, increasing trend (Fig. 1k), or no significant temporal trend (30.7%; Fig. 1l). The firing rates, on both laser and control trials, were stable across trial blocks in all three groups. The decreasing temporal trend was the most prevalent pattern within individual sessions (Fig. 1m). As the laser and control trial blocks are randomly interleaved, these results emphasize that the change in correlations is only observed in the differential response to optogenetic stimulation across time. That is, optogenetic stimulation is used to probe the state of the network at progressive time points. To further establish that the observed temporal changes to correlation structure are seen on a population scale (rather than being dominated by strong effects in a small number of pairs), we shuffled the pair identity within each trial block and recalculated the temporal correlation for vectors composed of correlations from randomized pairs (Fig. 1n). In this way, we shuffled the pair identity in each trial block, but preserved the temporal order across blocks. Notably, we found that the decreasing temporal trend was the dominant trend across the neural population. These results demonstrate that the decorrelation of synchronously active neurons is the general, dominant trend in visual cortical networks.

As correlations may limit encoded information[23] and constrain task performance[24], we further examined whether this dynamic change in correlation structure impacted the number of correct behavioral responses during the detection task. Overall, there was no difference in correct responses between laser and control trials ($P = 0.92$ paired Wilcoxon signed rank test, $n = 20$ sessions). However, monkeys made more correct responses on late trial blocks with laser stimulation when correlations were reduced, compared to early trials when correlations were elevated (c0 condition; 6.9% ±3.9 increase on laser versus control trials, mean ± s.e.m.; Fig. 1o, $P = 0.017$, Wilcoxon signed rank test, first versus last 14 trials). This behavioral improvement cannot be attributed to practice effects, as they did not occur in early versus late control trials, indicating that the change in correlations in laser trials contributed to the behavioral improvement. Further, we examined whether optogenetic stimulation could produce visible phosphenes that monkeys learned to ignore across sessions. We found no differences in the false alarm rates between laser and control trials on early or late trial blocks (Extended Data Fig. 1k,l). We calculated the ratio of false alarms on laser and control trials (FA ratio = laser FA/control FA) across chronologically ordered sessions, but found no noticeable temporal trend (Extended Data Fig. 1m; Pearson $R = 0.3$, $P = 0.1$; if animals were learning to ignore optogenetic stimulation, we would expect a decreasing trend across sessions). This is consistent with our previous findings[24,25] that optogenetic stimulation is not strong enough to produce readily detectable phosphenes. Thus, the dynamic decorrelation on progressive laser stimulation trials corresponds with a subtle, but significant, improvement in behavioral performance.

To determine whether the frequency of laser stimulation is critical to the temporally decreasing correlations, we performed additional experiments using multiple stimulation frequencies within a recording session. The duty cycle was adjusted so that the total 'laser on' time was maintained constant at 100 ms per trial (Fig. 2a). Each frequency block comprised at least 96 trials (first block 117.8 ± 11.9 trials; second block 161.7 ± 34.4 trials, mean ± s.e.m.; $n = 11$ sessions). All three frequencies tested produced a robust increase in firing rates (Fig. 2b). When all blocks were grouped together regardless of their temporal order, both 10 Hz (Fig. 2c) and 20 Hz stimulations (Fig. 2d) reduced correlations compared to control (similar to late trials at 35 Hz; Fig. 1f,g). However, when sessions were grouped based on their temporal recording order (Fig. 2a), regardless of stimulation frequency (Fig. 2a,e), the decreasing correlation patterns reemerged (Fig. 2f,g). Examining the first 20 trials of the first and second stimulation blocks revealed that on the first block, correlations on laser trials were elevated compared to control, but by the start of the second block, correlations were decreased in laser trials (Fig. 2h, $P = 2.0 \times 10^{-12}$, Kruskal–Wallis test, df = 3; and see also Extended Data Fig. 6 for similar results in the absence of 35 Hz sessions). Both the first and second stimulation blocks evoked significant increases in firing rates of neurons above control levels (Fig. 2i, $P = 1.3 \times 10^{-14}$, Kruskal–Wallis test, df = 3). Thus, randomization of the stimulation frequency was still able to produce a reduction in network interactions over time to indicate that the specific stimulation frequency is less important than the number of stimulation cycles.

Compensatory plasticity depends on brain state

Mechanisms of synaptic plasticity and associated changes in correlations can be highly dependent on brain state[26,27]. We thus examined whether the rapid compensatory plasticity revealed here is state-dependent by comparing the strength of plasticity between wakefulness and rest. Daily recording sessions consisted of a stimulus detection task (Fig. 3a, awake condition) similar to that in Fig. 1b, and a rest period (Fig. 3h; rest duration was 26.7 ± 2.2 min, mean ± s.e.m.) where lights were turned off and the animal had its eyes closed (rest was validated using the low-to-high frequency power ratio (PR) of the local field potential (LFP[28]; Methods). We use the term rest, rather than sleep, as we did not explicitly measure the sleep stages (see Methods for further details). Notably, the same cell population was monitored during both awake and rest conditions. During rest, optogenetic stimulation was delivered at the same frequency and duration (35 Hz, 10-ms width, 10 cycles per trial) and for similar numbers of trials as during wakefulness (awake sessions had 189.4 ± 36.8 trials, mean ± s.e.m.; rest session had 175.6 ± 18.4 trials; Extended Data Fig. 4d–f). As expected[26,29], rest reduced baseline firing rates relative to wakefulness (Fig. 3e; 78.1% decrease, control trials) and increased correlations (Fig. 3f; 44.4% increase, control trials).

Neuronal responses evoked by optogenetic stimulation were elevated both during rest and wakefulness (rest: 4.47 ± 0.15 sp s^{-1}, mean ± s.e.m., laser versus baseline; wakefulness: 4.97 ± 0.29 sp s^{-1}, $P = 0.1$, t-test between groups). During wakefulness, correlations initially increased and then decreased in early versus late trial blocks relative to control (Fig. 3b–d), as originally reported in Fig. 1. The transition in the strength of correlations during laser stimulation relative to control occurred near block 25 (Fig. 3d), with 46.7% of pairs exhibiting this behavior (Fig. 3d, inset). However, during rest, the optogenetic activation of the same neural population increased correlations throughout all trial blocks (Fig. 3h–k). Comparing the first and last blocks (Fig. 3k), there was a small decrease in the stimulation-evoked correlation change over time (correlation difference was 0.098 ± 0.0057 on the first trial block, versus 0.077 ± 0.0057 on the last trial block, mean ± s.e.m.; $P = 4.79 \times 10^{-4}$, Wilcoxon signed rank test). Similarly, during rest, the majority of cell pairs (59.3%) showed no significant, systematic temporal trend on laser trials (Fig. 3k, inset, same criteria as Fig. 1j–m). Examining the subset of cells on channels that were light-responsive both during wakefulness and rest exhibited similar results as the larger population (Extended Data Fig. 3d). Further, because rest sessions chronologically followed awake sessions, it should be noted that correlations increased during rest (Fig. 3f), so the difference in correlation dynamics between rest (Fig. 3k) and wakefulness (Fig. 3d) cannot be attributed to the network already being in a decorrelated state from the preceding awake stimulation. These results demonstrate that the compensatory process that progressively

https://doi.org/10.1038/s41593-023-01446-w

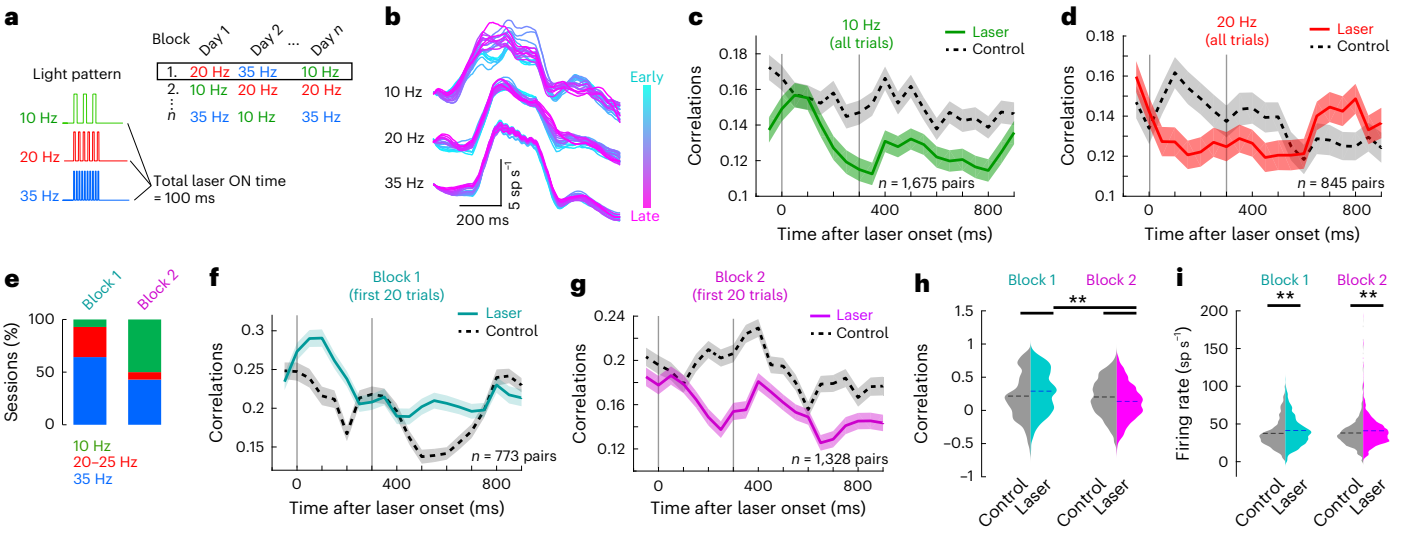

Fig. 2 | Stimulation cycles, not frequency, lead to temporally decreasing correlations. a, Experiments using different stimulation frequencies. On individual recording days (upper right, columns), monkeys performed multiple iterations of the stimulus detection task with laser stimulation delivered at different frequencies (upper right, rows; left panels). Note that here a 'block' refers to a set of trials with the same stimulation frequency. **b**, All laser stimulation frequencies produced significantly increased firing rates of neural populations consistently across early to late trial blocks (20 trials per block). **c**, Correlations across all sessions using 10-Hz stimulation. Lines show mean and envelope shows s.e.m. for laser (green) and control (black) trials. Vertical gray lines denote laser onset and offset. **d**, Same conventions as **c**, but for sessions using 20-Hz stimulation. **e**, Distributions of frequencies included in block 1 (left, $n = 11$ sessions) and block 2 (right, $n = 11$ sessions). **f**, Correlations of neuron pairs during the first 20 trials of the first trial block of each recording day in laser (blue) and control (black) trials. Data show population mean ± s.e.m. **g**, Same conventions as **f**, but for the first 20 trials of the second frequency block across all days. **h**, Correlations are significantly increased in the first block of trials on laser compared to control trials. In the second block of trials, laser stimulation induces a significant decrease in correlations ($^{**}P = 2.0 \times 10^{-12}$, Kruskal–Wallis test, df = 3, post hoc signed rank test for within block comparisons, rank-sum test for across block comparisons; $n = 765$ pairs). Dashed lines show means. **i**, Firing rates (geometric pair mean) are significantly higher in laser trials compared to control on both blocks 1 and 2 ($^{**}P = 1.3 \times 10^{-14}$, Kruskal–Wallis test, df = 3, same post hoc conventions as **h**; $n = 765$ pairs).

dampens network connectivity in response to repeated stimulation during wakefulness is substantially weakened during the resting state.

This striking state-dependent difference in the strength of rapid compensatory plasticity provides an important clue about the underlying mechanism of these network interaction changes. Specifically, we reasoned that even though the position of the recording array was held constant between wakefulness and rest, there were more laser-responsive neurons in the rest condition, and correlations were increased compared to wakefulness (Fig. 3e,f), indicating that neural populations operate under a different regime during rest. Indeed, it has been proposed that one major difference between these two brain states is a relative shift toward inhibition during wakefulness[30,31]. This raises the possibility that changes in inhibitory cell populations could underlie the compensatory plasticity observed in the awake state.

Large-scale network model

We investigated the underlying mechanism for the state-dependent temporal changes in neuronal interactions revealed here by developing a balanced, recurrent computational network[32] modeling homeostatic inhibitory (*I*) and excitatory (*E*) plasticity (Fig. 4a). The network was composed of 10,000 excitatory and inhibitory neurons, and compensatory plasticity was implemented by activity-dependent changes of inhibitory-to-excitatory (*I*–*E*) synapses[5]. Model optogenetic stimulation followed the temporal pattern used in vivo and uniformly increased the firing rates of 50% of the *E* neurons (Fig. 4b; see Methods for details). Consistent with experimental findings, the strength of correlations underwent a dynamic reversal following repeated activation across early to late trials (Fig. 4c–f). The dynamic change in correlations was a consequence of the light-induced potentiation of *I*–*E* synapses (Fig. 4g–i), which maintained *E* firing rates near a target firing rate, prescribed by the inhibitory weight update rule[5]. Thus, in response to optogenetic stimulation, compensatory *I*–*E* plasticity strengthened inhibitory feedback to ChR2-expressing cells and decorrelated their responses over the time course of the experiment[33–35]. Confirming experimental findings, the observed dynamic correlation reversal was independent of stimulation frequency (Extended Data Fig. 7) and was caused by a change in mean spike count covariances (rather than variances; Extended Data Fig. 7). Further, we tested several spike-timing dependent plasticity rules, but only the model implementing *I*–*E* plasticity could replicate the experimentally observed progressive decrease in correlations following optogenetic stimulation (Extended Data Fig. 8).

To verify model predictions that inhibitory plasticity drives experimentally observed changes in correlation structure, we divided our single units into broad (putative excitatory) and narrow spike waveform units (putative inhibitory; Fig. 4j)[36]. This allowed us to quantify the connection strength of simultaneously recorded pairs of neurons by measuring the area under the cross-correlogram (CCG) in early versus late control trials (potentiation index (PI); Methods). Only control trials were used to measure PI to exclude the synchronous activation due to optogenetic stimulation. The PI can be related to the measure of correlation under certain conditions (Methods), but in this context, the two measures can be considered independent; unlike correlations, the PI is calculated only on control trials using a shorter time interval. Consistent with the model, we found an increase in PI (potentiation) between the majority of putative *I*–*E* cell pairs (Fig. 4l; PI = 1.145 ± 0.1, mean ± s.e.m.) and a decrease in PI between most putative *E*–*E* pairs (Fig. 4k; PI = 0.988 ± 0.008, mean ± s.e.m.). Distributions of PIs were significantly different from unity for both groups (*E*–*E* pairs, $P = 0.04$, Wilcoxon signed rank test and *I*–*E* pairs, $P = 0.00097$, Wilcoxon signed rank test), and different from each other (*I*–*E* versus *E*–*E*, $P = 0.00024$, Wilcoxon rank-sum test).

Measuring the PI using a longer, 150 ms window yielded similar results (Extended Data Fig. 3e), with two distinctions. First, the longer window was able to identify more strongly potentiated *I*–*E*

https://doi.org/10.1038/s41593-023-01446-w

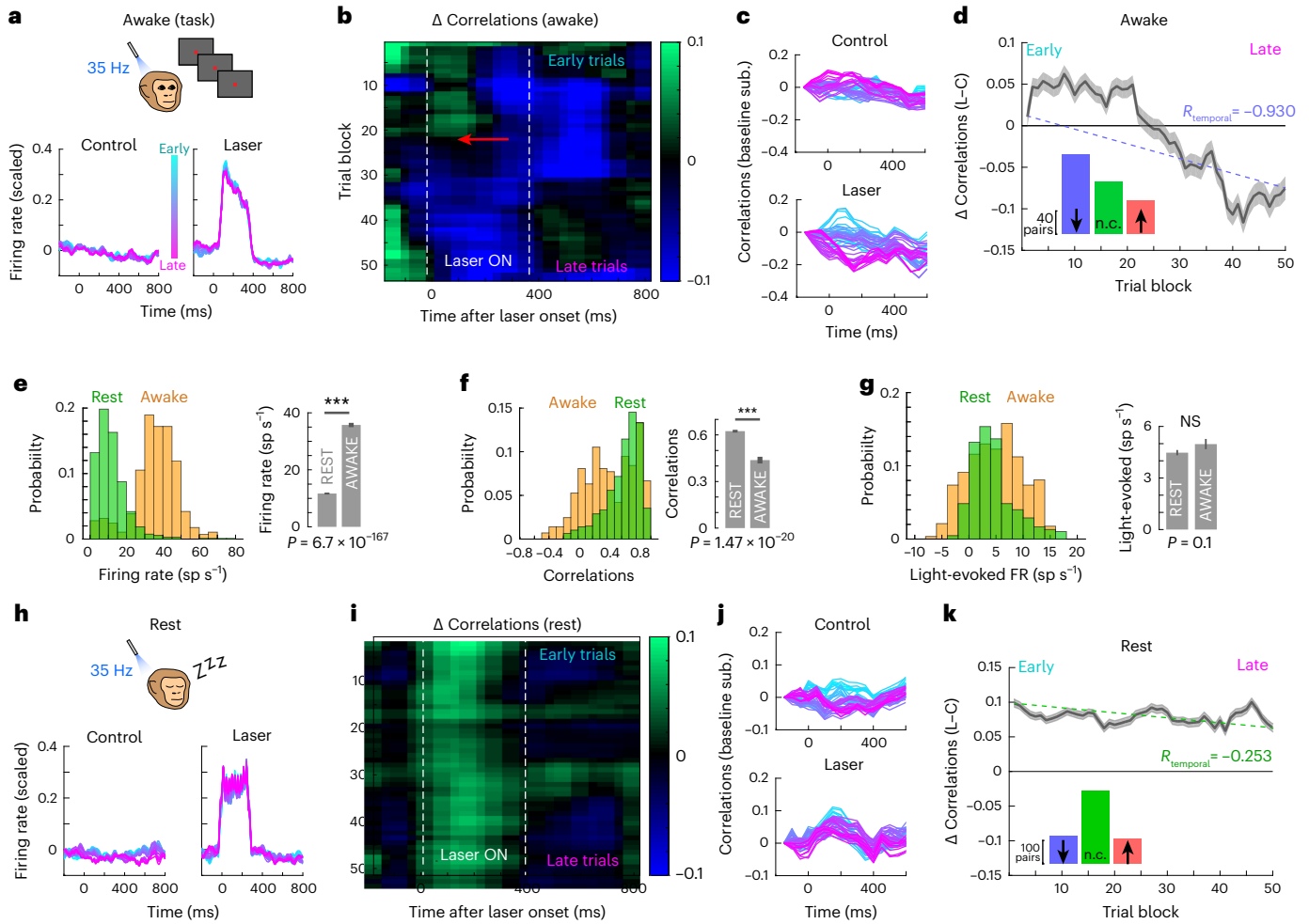

Fig. 3 | Reversal in neuronal correlations depends on behavioral state. **a**–**d**,**h**–**k**, Experiments using 35-Hz optogenetic stimulation during two behavioral states: awake detection task (**a**–**d**) and rest (**h**–**k**). **a**,**h**, Optical stimulation strongly increases firing rates of neural populations during the stimulus detection task (**a**) and rest (**h**) components. **b**,**i**, Correlation difference between laser and control trials during the awake (**b**, $n = 269$ pairs) and rest components (**i**, $n = 600$ pairs). Red arrow shows the transition from increased to decreased correlations only during the awake condition. **c**,**j**, Correlation change during laser stimulation compared to baseline state (200-ms window, before laser stimulation) across stimulation blocks during the awake (**c**) and rest (**j**) conditions. Baseline sub., baseline subtracted. **d**,**k**, Difference in correlations between laser and control across trial blocks (200 ms after laser onset) during awake (**d**) and rest (**k**) components. Data show population mean ± s.e.m. Dashed line connects the first and last trial blocks. Insets show counts of pairs with decreasing (blue), increasing (red) or no change (n.c.) in temporal trends (green). **e**–**g**, Rest resulted in a significant decrease in spontaneous firing rates compared to the awake condition (**e**, geometric mean, $P = 6.7 \times 10^{-167}$), and a significant increase in network correlations in the absence of optogenetic stimulation (**f**, $P = 1.47 \times 10^{-20}$). However, rest did not affect the amount of optogenetically evoked activity (**g**, $P = 0.1$). Bar plots (right) show mean and s.e.m. of rest and awake distributions (left). ***P values result from t-tests (two-tailed, unpaired) between distributions; $n = 711/285$ (rest/awake) pairs. NS, not significant.

pairs, which shifted the I–E PI distribution further to the right (potentiated). Conversely, for E–E pairs, the median of the PI distribution was still less than 1 (depressed), but was no longer significantly different from unity. Because stronger I–E potentiation was found with a longer PI time window, it is possible that I–E and E–E interactions occur on different timescales.

We further examined the time course of correlations between E–E and I–E pairs across cortical layers (Extended Data Fig. 9). The strongest PI (calculated using a 150-ms window centered on the CCG peak) was found between I–E pairs across supragranular and granular layers, and supragranular and infragranular layers. E–E pairs spanning supragranular and granular and within the granular layer were depressed (PI < 1). E–E pairs within the supragranular layer displayed the most variability in PI depending on the window size used to calculate the PI. Using a 150-ms window, supragranular E–E pairs were slightly but significantly potentiated (Extended Data Fig. 9c, left; median PI = 1.01, $P = 0.0046$). However, at shorter timescales (15-ms window around the peak) supragranular E–E pairs were slightly but significantly depressed (median PI = 0.99, $P = 0.019$). All other types of pairs showed similar PI distribution trends regardless of the time window used for calculation. Together, these results substantiate that rapid compensatory processes are mediated by dynamic changes in I–E synapses, particularly between supragranular and lower layers, consistent with model predictions[5].

Finally, sleep has been shown to lead to a net reduction in the strength of excitatory synapses[27], and hence we modeled 'rest' by downscaling all model synapses by 60% (Fig. 4m and Extended Data Fig. 10). This reduction in network weights was best able to replicate the experimental findings during rest (Fig. 4f and see also Extended Data Fig. 10 for 50% reduction). During rest, overall correlations in laser trial blocks remained greater than those in control (Fig. 4f), and there was a slight reduction in correlated responses across early to late laser trial blocks (Fig. 4n,o). Both observations are consistent with our experimental findings (Fig. 3h–k) and can be explained by decreased

inhibitory feedback from weaker *I*–*E* synapses during rest compared to wakefulness (Fig. 4i, magenta versus gold lines, respectively).

Discussion

In agreement with theoretical predictions[4], we provide the first experimental evidence, to the best of our knowledge, of a rapid form of plasticity that reduces, rather than increases, network connection strengths when excitatory neurons are repeatedly co-activated. Notably, we demonstrate that this compensatory process operates on the timescale of minutes, much faster than previously described forms of homeostatic plasticity. This form of compensatory plasticity primarily operates during wakefulness, but not sleep, when the brain is continuously bombarded with sensory information that could potentially saturate network connectivity in the absence of a rapid homeostatic process. Mechanistically, we suggest that this compensatory process depends on *I*–*E* plasticity, thus supporting previous computational studies[2,5,37,38] proposing that inhibitory plasticity has a critical role in stabilizing network dynamics in vivo.

Intuitively, repeated optogenetic stimulation of presynaptic, excitatory neurons will activate many postsynaptic targets to increase, rather than decrease, the strength of neuronal connectivity via associative plasticity mechanisms[21]. This is because blue light scatters rapidly in the brain tissue[39,40], and direct activation of transduced neurons is expected to primarily occur within ~200 µm (ref. 24), at the spatial scale of the light source. The light-evoked activity could propagate across much larger distances due to such multisynaptic activation[24]. Surprisingly, however, network-scale connectivity progressively decreased across trial blocks (Fig. 1g), and connectivity between putative excitatory cells decreased (Fig. 4k). Further, this reversal of correlations occurs regardless of whether we considered only pairs of neurons that are directly or indirectly modulated by light (Extended Data Fig. 3b). This is indicative of a process that induces changes on a network-wide scale and is not restricted solely to the most synchronously active cells. The overall decline in correlations reported here can be attributed to the progressive strengthening of connectivity between inhibitory and excitatory cells (Fig. 4g,l). This is the likely reason why induction of associative plasticity is more effective under inhibitory blockade[41,42].

The essential role of inhibitory plasticity in our model is similar to previous models describing rapid compensatory plasticity[5]. We show that *I*–*E* synaptic weights only need to be moderately increased to provide the necessary compensation (Fig. 4i), which may explain why this process is so rapid. Further, our findings are consistent with the proposed role of homeostatic plasticity in maintaining neural networks within an optimal dynamical regime. Homeostatic processes have been proposed to maintain firing rate stability by either scaling synapses[3] or modifying the threshold required to induce Hebbian plasticity ('sliding threshold model'). Both of these processes have been hypothesized to alter the excitatory–inhibitory balance[6], with synaptic scaling occurring following extreme changes in activity (that is, sensory deprivation), and sliding threshold mechanisms thought to be prevalent at more moderate activity changes in mature animals[7]. Such compensatory mechanisms may first act on correlations at short timescales and on firing rates at longer timescales.

While our results clearly demonstrate a change in the measured network response to optogenetic stimulation, further experiments using different experimental approaches are required to determine how our results relate to synaptic level changes. Two recent studies have shown that network correlations are influenced in a similar manner as firing rates during long-term homeostatic plasticity. Reference 15 showed that after sensory deprivation, network correlations return to baseline after 24 h, and ref. 16 showed that during this time, network-related synapses undergo tumor necrosis factor α-dependent increases in activity, while sensory-driven synapses do not. Future experiments are needed to determine whether a similar mechanism is responsible for both long-term homeostatic plasticity and the rapid network changes observed in our study. Critically, our results are not readily explainable by phenomena such as rapid firing rate adaptation or stimulus repetition suppression. The cellular and network mechanisms for rapid firing rate adaptation and stimulus repetition[43] suppression are still unclear. A key feature of both phenomena is that evoked firing rates are reduced in time. However, we found no substantial change in firing rates over time, in response to either optogenetic stimulation or visual stimuli. The stability of firing rates suggests that our results are unlikely to be explained by postsynaptic receptor downregulation, or exhaustion of presynaptic vesicles, although we cannot rule out a complex combination of these factors. In relation to stimulus repetition suppression, Brunet et al. found that strong visual stimuli can modulate gamma-band coherence in monkey visual cortex, with differential effects on the population of putative inhibitory interneurons and pyramidal neurons. The study in ref. 43 suggested that inhibitory neurons are responsible for increasing gamma-band synchrony in the network. While our optogenetic stimulation does synchronously increase the firing of a subset of directly activated glutamatergic neurons, the evoked firing rates are much lower than those evoked by large, high-contrast visual stimuli. Notably, findings in ref. 43 applies to the time period of 0.3 s after stimulus onset. Further investigations are required to determine whether the correlation changes observed in our study may be related to gamma-band synchrony during stimulation. Unfortunately, due to strong light-induced artifacts in the LFP signal[44], we were unable to perform this comparison using our dataset.

An important consideration in the interpretation of our results is that fluctuations in behavioral state[45] or eye movements[46] could impact correlations. In this respect, we considered the possibility that optogenetic stimulation could have induced a perceivable phosphene that animals learned to ignore across time. However, when we measured false alarm patterns, both within and across sessions, as well as various eye movement parameters across time, and between laser and control trials (Extended Data Fig. 1), we found no indication that this was the case. Nonetheless, while our current results do not

Fig. 4 | Model simulations with *I*–*E* plasticity replicate experimental findings. **a**, Recurrent network of 8,000 *E* and 2,000 *I* cells, driven by an external feed-forward layer of Poisson neurons of 10-Hz rate and 0.1 pairwise correlations, connecting to 10% of all neurons. Only inhibitory-to-excitatory synapses were plastic; 4,000 *E* neurons were driven during 'laser' trials. **b**, Change in mean firing rate (laser minus control) over trials. **c**, Change in mean correlations (laser minus control) over trials. **d**, Change in mean correlations during laser trials compared to the first time-bin over the time course of a trial. **e**, Change in mean correlations averaged over light-driven pairs and over realizations of the connectivity matrix. Error bars indicate a 95% confidence interval. Light blue indicates block 1, blue is block 10 and dark blue represents block 40. **f**, Change in mean pairwise correlations at the center time-bin of the laser stimulation period ($t = 250$ ms) across trials averaged over nine realizations of the connectivity matrix. Error bars indicate a 95% confidence interval. Golden line corresponds to the network in the rest state ($f = 0.4$). Magenta line corresponds to the awake state ($f = 1$). **g**, Percent change of mean synaptic weight compared to baseline (first time-bin) during laser trials. **h**, Same as **g**, but for control trials. **i**, Evolution of the mean *I*–*E* synaptic weight over the course of the entire experiment in awake and rest conditions. Shaded area indicates standard error. Inhibitory weights are potentiated due to repeated activation of *E* cells. **j**, Left, PI was calculated for all pairs of broad (green) and narrow (purple) single unit pairs on control trials. Right, example raw CCG for one narrow–broad waveform pair on early (upper) and late (lower) trials. **k**, Distribution of all PIs for all broad waveform pairs ($n = 1{,}382$). Arrowhead shows median. **l**, Distribution of all PIs for all broad–narrow waveform pairs ($n = 94$). Arrowhead shows median. **m**, Same as **a**, but during rest; all synapses are downscaled by factor *f*. **n**, Same as **d**, but during rest condition. **o**, Same as **e**, but during rest condition. Panels **j**–**l** show experimental results; remainder show modeling results. Gray shaded regions in panels **d**, **e**, **g**, **n** and **o** denote the time interval of light presentation.

https://doi.org/10.1038/s41593-023-01446-w

indicate any observable changes in animals' behavior over the course of a session that could account for the temporal trends in correlations on laser trials, we cannot completely exclude the possibility that a more subtle, and difficult-to-detect, behavioral shift might occur. However, this is unlikely because our computational model, which only relies on interactions between excitatory and inhibitory neurons in the absence of behavioral-induced modulations, exhibits similar temporal dynamics in correlation structure as the experimental data.

Our measure of dynamic correlations within a neural population using a light-probing stimulus provides a new method for detecting rapid, network-scale plasticity, which would otherwise be impossible to detect by examining firing rates alone. This simple population measure

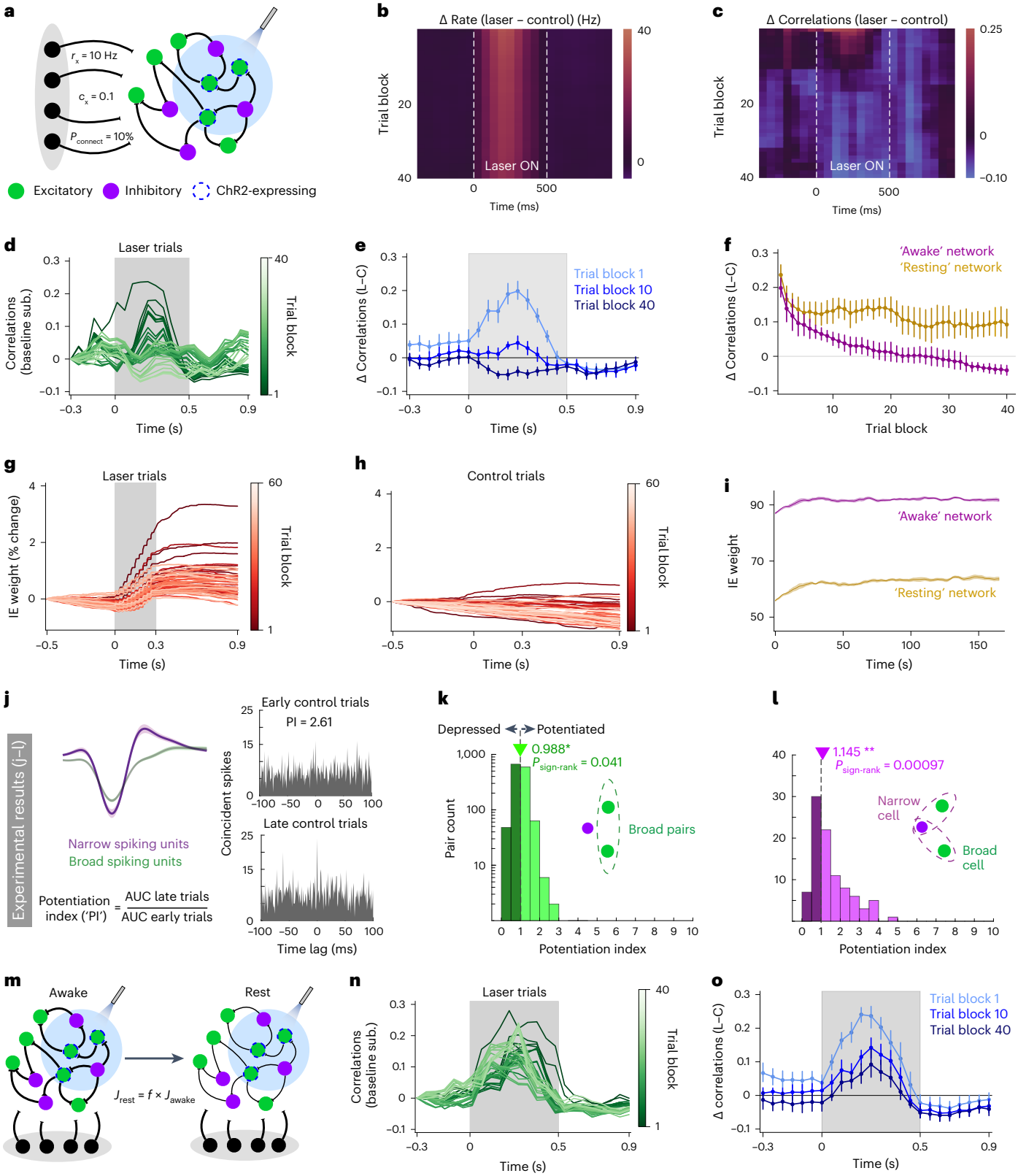

of network plasticity can be readily applied to awake, in vivo recordings, where multiple, paired whole-cell recordings—more commonly used in plasticity studies—pose a difficult technical challenge. Finally, we present the first experimental and analytical evidence in favor of a rapid, inhibition-driven, compensatory process that decorrelates neuronal responses in vivo. Along with adaptation and divisive inhibition, this is one of the mechanisms that acts to keep cortical circuits near their ideal operating point despite changes in exogenous input, strengthened connections between pyramidal cells, or neuromodulators[47]. As this compensatory process is substantially weakened during rest (Fig. 3), an intriguing prediction is that associative plasticity would be easier to induce during sleep when prompted by external stimulation.

Online content

Any methods, additional references, Nature Portfolio reporting summaries, source data, extended data, supplementary information, acknowledgements, peer review information; details of author contributions and competing interests; and statements of data and code availability are available at https://doi.org/10.1038/s41593-023-01446-w.

References

1. Abbott, L. F., Varela, J. A., Sen, K. & Nelson, S. B. Synaptic depression and cortical gain control. *Science* **275**, 220–224 (1997).
2. Zenke, F. & Gerstner, W. Hebbian plasticity requires compensatory processes on multiple timescales. *Philos. Trans. R. Soc. Lond. B Biol. Sci.* **372**, 20160259 (2017).
3. Turrigiano, G. G. The self-tuning neuron: synaptic scaling of excitatory synapses. *Cell* **135**, 422–435 (2008).
4. Zenke, F., Gerstner, W. & Ganguli, S. The temporal paradox of Hebbian learning and homeostatic plasticity. *Curr. Opin. Neurobiol.* **43**, 166–176 (2017).
5. Vogels, T. P., Sprekeler, H., Zenke, F., Clopath, C. & Gerstner, W. Inhibitory plasticity balances excitation and inhibition in sensory pathways and memory networks. *Science* **334**, 1569–1573 (2011).
6. Keck, T., Hü Bener, M. & Bonhoeffer, T. Interactions between synaptic homeostatic mechanisms: an attempt to reconcile BCM theory, synaptic scaling, and changing excitation/inhibition balance. *Curr. Opin. Neurobiol.* **43**, 87–93 (2017).
7. Lee, H. K. & Kirkwood, A. Mechanisms of homeostatic synaptic plasticity in vivo. *Front. Cell. Neurosci.* **13**, 520 (2019).
8. El-Boustani, S. et al. Locally coordinated synaptic plasticity of visual cortex neurons in vivo. *Science (1979)* **360**, 1349–1354 (2018).
9. Mainen, Z. F. & Seinowski, T. J. Reliability of spike timing in neocortical neurons. *Science* **268**, 1503–1506 (1995).
10. Doiron, B., Litwin-Kumar, A., Rosenbaum, R., Ocker, G. K. & Josić, K. The mechanics of state-dependent neural correlations. *Nat. Neurosci.* **19**, 383–393 (2016).
11. Yatsenko, D. et al. Improved estimation and interpretation of correlations in neural circuits. *PLoS Comput. Biol.* **11**, e1004083 (2015).
12. Cohen, M. R. & Kohn, A. Measuring and interpreting neuronal correlations. *Nat. Neurosci.* **14**, 811–819 (2011).
13. Smith, M. A. & Kohn, A. Spatial and temporal scales of neuronal correlation in primary visual cortex. *J. Neurosci.* **28**, 12591–12603 (2008).
14. Hansen, B. J., Chelaru, M. I. & Dragoi, V. Correlated variability in laminar cortical circuits. *Neuron* **76**, 590–602 (2012).
15. Wu, Y. K., Hengen, K. B., Turrigiano, G. G. & Gjorgjieva, J. Homeostatic mechanisms regulate distinct aspects of cortical circuit dynamics. *Proc. Natl Acad. Sci. USA* **117**, 24514–24525 (2020).
16. Barnes, S. J., Keller, G. B. & Keck, T. Homeostatic regulation through strengthening of neuronal network-correlated synaptic inputs. *eLife* **11**, e81958 (2022).
17. Bair, W., Zohary, E. & Newsome, W. T. Correlated firing in macaque visual area MT: time scales and relationship to behavior. *J. Neurosci.* **21**, 1676–1697 (2001).
18. Han, X. et al. Millisecond-timescale optical control of neural dynamics in the nonhuman primate brain. *Neuron* **62**, 191–198 (2009).
19. Johansen, J. P. et al. Optical activation of lateral amygdala pyramidal cells instructs associative fear learning. *Proc. Natl Acad. Sci. USA* **107**, 12692–12697 (2010).
20. Malenka, R. C. Postsynaptic factors control the duration of synaptic enhancement in area CA1 of the hippocampus. *Neuron* **6**, 53–60 (1991).
21. Erickson, M. A., Maramara, L. A. & Lisman, J. A single brief burst induces GluR1-dependent associative short-term potentiation: a potential mechanism for short-term memory. *J. Cogn. Neurosci.* **22**, 2530–2540 (2010).
22. Bliss, T. V. P. & Lømo, T. Long-lasting potentiation of synaptic transmission in the dentate area of the anaesthetized rabbit following stimulation of the perforant path. *J. Physiol.* **232**, 331–356 (1973).
23. Moreno-Bote, R. et al. Information-limiting correlations. *Nat. Neurosci.* **17**, 1410–1417 (2014).
24. Andrei, A. R., Pojoga, S., Janz, R. & Dragoi, V. Integration of cortical population signals for visual perception. *Nat. Commun.* **10**, 3832 (2019).
25. Andrei, A. R. et al. Heterogeneous side effects of cortical inactivation in behaving animals. *eLife* **10**, e66400 (2021).
26. Ecker, A. S. et al. State dependence of noise correlations in macaque primary visual cortex. *Neuron* **82**, 235–248 (2014).
27. Vyazovskiy, V. V., Cirelli, C., Pfister-Genskow, M., Faraguna, U. & Tononi, G. Molecular and electrophysiological evidence for net synaptic potentiation in wake and depression in sleep. *Nat. Neurosci.* **11**, 200–208 (2008).
28. Beaman, C. B., Eagleman, S. L. & Dragoi, V. Sensory coding accuracy and perceptual performance are improved during the desynchronized cortical state. *Nat. Commun.* **8**, 1308 (2017).
29. Scholvinck, M. L., Saleem, A. B., Benucci, A., Harris, K. D. & Carandini, M. Cortical state determines global variability and correlations in visual cortex. *J. Neurosci.* **35**, 170–178 (2015).
30. Haider, B., Häusser, M. & Carandini, M. Inhibition dominates sensory responses in the awake cortex. *Nature* **493**, 97–100 (2013).
31. Bridi, M. C. D. et al. Daily oscillation of the excitation-inhibition balance in visual cortical circuits. *Neuron* **105**, 621–629 (2020).
32. Akil, A. E., Rosenbaum, R. & Josić, K. Balanced networks under spike-time dependent plasticity. *PLoS Comput. Biol.* **17**, e1008958 (2021).
33. Stringer, C. et al. Inhibitory control of correlated intrinsic variability in cortical networks. *eLife* **5**, e19695 (2016).
34. Tetzlaff, T., Helias, M., Einevoll, G. T. & Diesmann, M. Decorrelation of neural-network activity by inhibitory feedback. *PLoS Comput. Biol.* **8**, e1002596 (2012).
35. King, P. D., Zylberberg, J. & Deweese, M. R. Inhibitory interneurons decorrelate excitatory cells to drive sparse code formation in a spiking model of V1. *J. Neurosci.* **33**, 5475–5485 (2013).
36. Ardid, S. et al. Mapping of functionally characterized cell classes onto canonical circuit operations in primate prefrontal cortex. *J. Neurosci.* **35**, 2975–2991 (2015).
37. Hennequin, G., Agnes, E. J. & Vogels, T. P. Inhibitory plasticity: balance, control, and codependence. *Annu. Rev. Neurosci.* **40**, 557–579 (2017).
38. Naumann, L. B. & Sprekeler, H. Presynaptic inhibition rapidly stabilises recurrent excitation in the face of plasticity. *PLoS Comput. Biol.* **16**, e1008118 (2020).

39. Yizhar, O., Fenno, L. E., Davidson, T. J., Mogri, M. & Deisseroth, K. Optogenetics in neural systems. *Neuron* **71**, 9–34 (2011).
40. Li, N. et al. Spatiotemporal constraints on optogenetic inactivation in cortical circuits. *eLife* **8**, e48622 (2019).
41. Wigström, H. & Gustafsson, B. Facilitated induction of hippocampal long-lasting potentiation during blockade of inhibition. *Nature* **301**, 603–604 (1983).
42. Feldman, D. E. E. The spike-timing dependence of plasticity. *Neuron* **75**, 556–571 (2012).
43. Brunet, N. M. et al. Stimulus repetition modulates gamma-band synchronization in primate visual cortex. *Proc. Natl Acad. Sci. USA* **111**, 3626–3631 (2014).
44. Mikulovic, S. et al. On the photovoltaic effect in local field potential recordings. *Neurophotonics* **3**, 015002 (2016).
45. Cohen, M. R. & Maunsell, J. H. R. Attention improves performance primarily by reducing interneuronal correlations. *Nat. Neurosci.* **12**, 1594–1600 (2009).
46. McFarland, J. M., Cumming, B. G. & Butts, D. A. Variability and correlations in primary visual cortical neurons driven by fixational eye movements. *J. Neurosci.* **36**, 6225–6241 (2016).
47. Froemke, R. C. Plasticity of cortical excitatory-inhibitory balance. *Annu. Rev. Neurosci.* **38**, 195–219 (2015).

Methods

Animal subjects

All experiments were performed in accordance with protocols approved by The Animal Welfare Committee (AWC) and the Institutional Animal Care and Use Committee (IACUC) for McGovern Medical School at The University of Texas Health Science Center at Houston. Two male rhesus monkeys (*M. mulatta*), ages 22 years (M2) and 16 years (M1) at the start of experiments, were implanted with a headpost and a 19-mm titanium chamber (Crist Instruments) over primary visual cortex (V1). A second chamber was implanted in monkey 2 over V1 on the contralateral hemisphere.

Viral vector preparation and injection

The gene for 'ChR2' was expressed specifically in V1 excitatory cells using the same viral construct as in ref. 48. VSVg-pseudotyped lentivirus carrying the genes for ChR2-GFP under the control of the α-CaMKII promoter. High titer (>10^9 IU ml^{-1}) purified lentivirus was obtained from the University of North Carolina Gene Therapy Center Vector Core. The virus was injected through a 29-gauge needle connected via mineral oil-filled tubing to a Hamilton syringe mounted on a perfusion pump (KD Scientific). The needle was advanced by a precision, computer-controlled microdrive (NAN Instruments) to a pre-established depth (corresponding to the lowest depth at which unit activity was found in preliminary experiments). After a 15-min waiting period (to achieve stability), 1 µl of virus suspension was delivered over a 10-min period. The needle was then retracted upward (0.1 mm min^{-1}) in 200–300 µm steps and an additional 1 µl of virus suspension was delivered at 3–4 additional depths. Five-minute wait periods were interleaved before and after each virus delivery and retraction step. Multiple injections were performed in each V1 chamber (8 for M1, and 11 and 4 for M2 in the right and left hemispheres, respectively) closely grouped together and forming a rectangular pattern across the cortical surface. We allowed at least 6 weeks for viral expression before electrophysiological experiments. Viral expression was long-lasting. We have observed robust light modulation months to years have the original injections.

Behavioral experiments

During each daily recording session, monkeys performed a series of tasks before the detection task to identify sites of light-responsive units, map receptive field locations and determine the preferred orientation of units. Monkeys sat in conventional primate chairs, head-restrained, in front of a computer monitor 90 cm away. Eye position was continuously monitored using an infrared, mirror-based eye tracking system operating at 1 kHz (EyeLink II, SR Research). Eye position and microsaccade analysis[48] are shown in Extended Data Fig. 1. Receptive field locations were mapped using 0.33° reverse correlation stimuli (full contrast, sinusoidal gratings and four orientations) presented at random screen locations. To initially identify light-responsive units, monkeys performed a fixation task with laser stimulation (24 Hz, 10 cycles and 10-ms width) on 50% of trials (total trials were typically 20–30). For the main detection task, monkeys fixated on a dark screen and 50% of trials presented gray-scale sinusoidal gratings of various luminance-varying contrasts. Stimuli were generated using MATLAB with Psychophysics Toolbox[49] and presented on a cathode ray tube screen on a dark background. Monkeys fixated throughout the trial on a central point (0.4° in size) within a 1° fixation window while stimuli with a diameter of 2–3° were displayed at 2–4° eccentricity. Monkeys signaled the presence or absence of a visual stimulus by holding (no stimulus) or releasing (stimulus present) a response bar. Correct behavioral responses were rewarded with five drops of juice. The trial structure is as follows: a visual cue was presented at the center of the screen. Animals were required to maintain stable fixation on the cue for 0.78–1.48 s, after which a visual stimulus of variable contrast was presented for 300 ms. Optogenetic stimulation was simultaneously applied for 285 ms (35 Hz), aligned to visual stimulus onset. After the stimulation period, animals continued fixating for an additional 1,000 ms to receive a juice reward. The location and size of the stimuli, when present, covered the multiple receptive fields of the cells recorded. Stimuli had a fixed spatial frequency (1.7 cycles per degree), displayed for 300, 800 or 1,300 ms, starting 450–1,000 ms after fixation onset. The orientation of the grating stimuli could vary both within and across sessions. In each experiment, stimuli could have one of four different luminance contrasts and were present in 50% of the trials. Peak (mean) luminance measurements for stimulus contrasts ranged between 0.107 (0.0935) and 0.280 (0.18) cd m^{-2}, while the minimum luminance and the no stimulus condition had a luminance of 0.08 cd m^{-2} (Tektronix, J17). The analysis presented here focuses on the 50% of trials in which no visual stimulus was present on the screen (contrast 0%). Some of the data presented here have been previously published, with a focus on the stimulus trials (see ref. 24 for further stimulus details). Optogenetic stimulation was triggered simultaneously with the onset of the visual stimuli (or at the time when a stimulus was expected, on no-stimulus trials). Optogenetic stimulation was present in 50% of trials. All stimulus and/or laser conditions were randomly interleaved. Each session consisted of 160–720 total trials. Behavioral performance was calculated as the percentage of correct stimulus reports of the total complete trials in each stimulus and optogenetic stimulation condition separately.

Rest experiments

For the rest experiments (Fig. 3e–h), following the behavioral task, animals were allowed to rest in a dark room for 18–40 min (26.7 ± 2.2 min, mean ± s.e.m.), during which electrophysiological recordings, optogenetic stimulation and eye tracking continued. During these rest periods, white noise was played through a speaker to dampen external sounds that might arouse the monkey. Animals had previously been acclimatized to take naps in the experiment room, and the timing of the rest experiments was carefully aligned to coincide with the time when monkeys naturally take daytime naps (approximately 2 pm). Rest was defined by two measures. First, a binary eye closure index was derived from the pupil signal (1 for eye closed, 0 otherwise), and only those sessions were included in which the eye closure index was 1 for more than 85% of the rest period. Second, we measured the presence of rest-associated slow wave activity by calculating a PR from the local field potentials. LFP PR was computed from the LFP power in the low-frequency bands (0.5–10 Hz) and LFP power in the high-frequency bands (30–80 Hz). PR was computed as follows: $PR = (P_{low} - P_{high})/P_{low}$, where P_{low} is the spectral power in the 0.5–10-Hz range, and P_{high} is the spectral power in the 30–80 Hz. Rest was considered to have been achieved if the rest condition had a significantly higher LFP PR than the awake ($P < 0.05$, Wilcoxon rank-sum test awake versus rest trials). As our experimental methods did not include polysomnography electrodes, we cannot quantitatively define the stage of sleep our rest periods achieved. However, based on observations of the animals' neural activity and facial expressions during rest, we would correlate 'rest' periods with sleep stages 1 or 2. Task and rest sessions ($n = 11$) shown in Fig. 3 were collected on the same day and the recording electrode position was maintained at the same site. During the task (rest), we recorded 125 (142) light-responsive units, resulting in 285 (711) pairs.

Electrophysiology

Extracellular recordings were performed with laminar electrodes (U-probe, Plexon) consisting of a linear array of 16–24 equally spaced contacts (100 µm intercontact spacing). Each platinum–iridium-coated electrode contact was 25 µm in diameter. The impedance at each contact typically ranged between 0.3 and 1.0 MΩ. Real-time extracellular neuronal spike waveforms (simultaneous 40 kHz analog-to-digital (A/D) conversion on each channel) were acquired using the Multichannel Acquisition Processor system (MAP system, 64 channel, Plexon).

Neural activity was amplified, filtered (low cutoff 0.7–100 Hz; high cutoff 300–8 kHz) and monitored online (Sort Client, Plexon) and through a speaker. We recorded 1,186 pairs of neurons from monkey 1 (21 sessions) and 1,227 pairs from monkey 2 (8 sessions).

Optogenetic stimulation

Light was delivered to neurons using a 100 mW, TTL-controlled, DPSS blue (473 nm) laser (RGBLase) coupled to a 200-µm diameter optical fiber, encased in stainless steel for structural rigidity. The fiber optic cable was independently controllable via the microdrive system (NAN Instruments). The light power at the tip of the fiber was within the range of 6.7–14.5 mW mm^{-2} (integrating sphere sensor, S124C Thor Labs) and was held constant across experiments. Before each experiment, at the bench, the fiber optic was aligned with the upper third of the electrode contacts. The shafts of both devices were marked with registration lines to provide a secondary measure of the vertical alignment of the fibers once the dura was penetrated. The fiber optic and recording electrode were lowered together, through a custom grid designed to minimize the distance between the optical fiber tip and the probe (range was ~0–300 µm, with most sessions having a spacing of ~100–200 µm; see ref. 24 for further details). For the majority of experimental sessions (Figs. 1 and 3a–d), light stimulation consisted of ten bursts of 10-ms light pulses at 35 Hz. The laser output was regulated via TTL pulses driven by a waveform generator (Model 3220A, Agilent Technologies), controlled by the experiment control module (FHC). For sessions in which the stimulation frequency was varied (Fig. 2), the total time the laser was on was kept constant at 100 ms per trial, and the frequency and duty cycle were modified accordingly. Laser power output was kept constant throughout. For rest sessions (Fig. 3e–h), stimulation parameters and laser power were unchanged from the awake condition (Fig. 3a–d).

Quantification and analysis methods

Cell and waveform classification. Spike sorting was performed offline using waveform-based principal component (PC) analysis software (Offline Sorter, Plexon). Single units were separated from multiunit activity based on the following two criteria: (1) unit cluster in PC space clearly separated from multiunit activity cluster and (2) waveforms with amplitudes that were 3 s.d. greater than the noise envelope. Units that did not meet these criteria but displayed significant responses to optogenetic stimulation were considered multiunit activity. Subsequent analysis was performed using custom MATLAB scripts (MATLAB 2016a, 2019a, Mathworks) and Microsoft Excel. Light-responsive units were functionally identified by comparing the firing rates on trials during the laser-on period (first 300 ms) with the equivalent period in the control trials in the absence of a visual stimulus (statistical criterion was $P < 0.05$, Wilcoxon rank-sum test). To classify waveforms into broad (putative excitatory) and narrow (putative inhibitory) units, for each well-isolated unit meeting the single unit criteria described above, averaged waveforms were aligned to the time of threshold crossing and each waveform was then interpolated (MATLAB, 'spline' function) to increase the temporal precision from 25 to 2.5 µs. Next, the mean trough-to-peak duration was measured, as waveform width is the single most robust characteristic to discriminate cell classes from extracellular recordings[35]. Trough-to-peak duration is the interval between the global minimum of the waveform curve and the subsequent local maximum. Narrow/broad spiking units were defined by a trough-to-peak duration less/greater than 200 µs. This threshold was chosen based on previous studies[35,36] and provides a conservative discriminant between the waveform width of parvalbumin-positive interneurons and other cell types[35].

Layer identification. To identify layers (Extended Data Fig. 9), current source density (CSD) analysis was performed[14,50,51]. Briefly, high-contrast stimulus-evoked responses in LFPs were recorded from equally spaced (100 µm) laminar contacts. Next, we computed the second spatial derivative of the evoked response potentials (iCSD toolbox for MATLAB[52]). The granular–infragranular layer boundary was identified by the lower bound of the earliest sink, measured in nA mm^{-3}. Channels located in the primary sink were identified as the granular layer (spanning three to four contacts). Channels above the sink were marked as the supragranular layer and channels below the sink were marked as the infragranular layer.

Dynamic noise correlations. To examine the dynamics of correlated variability, we divided our data into 200 ms windows within the time course of a trial (sliding every 50 ms) and in blocks of 20 trials (sliding every trial). Trials were ordered in chronological order separately for laser and control trials. A total of 20 trials per block was chosen as a compromise between accurate noise correlation estimates and providing sufficient blocks within a session to measure long-time course dynamics. For each time block, correlated variability was independently computed as described previously[14,24,28]. Briefly, spike counts for each pair of neurons in each time block were z-scored and the correlated variability was calculated using the Pearson correlation coefficient $R(x, y)$ given:

$$R(x,y) = \frac{\sum_{n=1}^{N} [x(n) - \bar{x}]\,[y(n) - \bar{y}]}{\sigma_x \sigma_y}$$

where n is the number of trials in the time block, $\bar{x}$ and $\bar{y}$ are the means of the spike counts of neurons x and y, respectively, and σ_x and σ_y are the s.d. of x and y, respectively. Correlated variability for all time blocks and laser/control conditions were calculated independently. Correlated variability was calculated for neurons that showed a significant response to the laser stimulation (see above) and had a mean firing rate ≥1 Hz. The laser responsiveness criteria were not included for narrow waveform pairs (Fig. 4j,l and Extended Data Fig. 9). We removed the trials in which the response of either cell in the pair was >3 s.d. above its individual mean[53]. Statistical comparisons were performed as stated in the text. Only sessions with a minimum of 59 trials in the no stimulus condition on both laser and control trials were included. Stimulus trials were excluded from all correlated variability analyses, as the presence of a visual stimulus can markedly alter correlation structures[24,54]. Otherwise, all data from both animals were included in these analyses.

Temporal trends. To quantify the temporal trends of correlations over time (that is, Fig. 1j–m), a Pearson correlation was calculated between sequentially calculated pairwise spike count correlation values and the trial block order. Pairs with absolute temporal correlations greater than 0.3 were considered significant. The reliability of Pearson correlations is very much dependent on the sample size used to calculate them. The threshold of 0.3 was chosen based on a statistical critical value table for the Pearson correlation, using the sample size (total trials used to calculate correlation) and an α value of 0.05. To test the robustness of the temporally decreasing correlations on laser trials evident in the entire population (Fig. 1g), for each session, the pairwise spike count correlations for simultaneously recorded pairs were shuffled within each trial block, thus preserving temporal trends, while destroying pair identity. Next, temporal correlations were calculated for each shuffled 'pair' on laser and control trials. The random number generator was reseeded for each session. One representative example of shuffled temporal trend distributions across all sessions is shown in Fig. 1n. The shuffle procedure was repeated 100 times (temporal correlations on laser trials median $R = -0.1686 \pm 0.0026$ s.d.; control trial median $R = 0.0756 \pm 0.0025$ s.d.). The majority of sessions (82%) displayed a clear reversal of correlations (like in Fig. 1g) with optogenetic stimulation across trial blocks (across sessions occurring at trial block 19 ± 2.2, mean ± s.e.m.). Some sessions (18%) showed only a progressive decrease in correlations, without the initial increase. For these

latter sessions, it is possible that the procedure for identifying the laser-responsive neurons took more trials (hence more stimulation), and the network was already entering the decorrelated state when the detection task begun.

PI. For each pair of single units, a cross-correlation (MATLAB 'xcorr' function, 'maxlags' = 200 ms) was performed using all spikes from control (no laser), no visual stimulus trials. Because the animals only maintained fixation on a dark screen during these trials, the entire trial duration (fixation start to reward onset) was used. Cross correlations ('CCGs') were performed for early and late trial blocks, each consisting of the first and last 20 trials. Only sessions with a minimum of 59 trials in this condition were included, as in the noise correlation calculations. The PI was defined for each pair of cells as the area under the CCG curve (measured over 15 or 150 ms on either side of zero lag; MATLAB 'trapz' function) on early trials, divided by the area under the CCG curve on late trials. Thus, if PI = 1, there is no difference in the number of joint spike events between early and late trials, while if PI < 1, there are fewer joint spikes in late trials ('depressed') and if PI > 1, there are more joint spikes on late trials ('potentiated'). All sessions had consistent waveform characteristics throughout the recording and contained mixtures of both depressed and potentiated pairs, indicating that differences in early versus late CCGs are not attributable to unstable recordings. The PI is loosely related to the measure of correlation. The PI is based on the area under the CCG. This relationship between the CCG and correlations was extensively studied in ref. 17. Briefly, the study in ref. 17 found that there was a strong correspondence between the area under the CCG and the correlation measure when correlations are calculated over the entire trial duration (2 s in their case). For time windows shorter than the trial duration, the relationship between the two measures is less predictable. Two important distinctions between the two measures in our study should be highlighted. First, unlike correlations, the PI is only measured using control (no optogenetic stimulation) trials to avoid the confound of synchronous, light-evoked coincident spikes. Second, the PI is calculated from CCGs obtained from the entire trial duration while animals fixated, unlike correlations that are measured in 200 ms sliding windows across trials.

Network model. The model is described in detail in the Supplementary Information. Briefly, we used a recurrent, balanced network composed of $n = 104$ exponential integrate-and-fire neurons, 80% of which were excitatory (E) and 20% inhibitory (I), receiving feed-forward synaptic input from an external population of excitatory neurons (Fig. 4a). To calculate dynamic correlations in the same manner as the experimental data, the trial-based design was replicated in the model simulations. Each trial in the simulation was 1.4 s long. To model the optogenetic stimulation, half of the excitatory neurons were stimulated by providing input in pulses of width 10 ms, at 35 Hz, and 10 cycles. The laser onset was at 500 ms and lasted for 300 ms, and was present in half of the trials (laser trials). We modeled the input as a collection of Poisson spike trains with rates $r_X = 10$ Hz, and pairwise correlations $c_X = 0.1$ (thus the network is in a correlated state). The synaptic weights were scaled with network size as $1/\sqrt{N}$, and the network was randomly connected. We modeled plasticity-induced changes in the synaptic weights using spike trains and eligibility traces.

Statistics and reproducibility

No statistical methods were used to predetermine sample sizes, but our sample sizes are similar to those reported in previous publications using similar experimental procedures[14,24,55]. Investigators were not blinded to experimental groups due to the nature of the experiments. However, all conditions were randomized in each experimental session—all conditions were present in both animals—and data were grouped automatically in MATLAB, without investigator intervention. We generally used nonparametric statistical tests, which do not assume normality. For other tests, data distributions were plotted and assumed to be normal but normality was not formally tested.

Reporting summary

Further information on research design is available in the Nature Portfolio Reporting Summary linked to this article.

Data availability

All source data used to generate experimental figures are available at https://zenodo.org/record/7527435.

Code availability

Parameters used for model simulations are provided in the Supplementary Information (Table 1). Model code is available at https://github.com/alanakil/optogenetic_corr_modulation/.

References

48. Hafed, Z. M., Lovejoy, L. P. & Krauzlis, R. J. Modulation of microsaccades in monkey during a covert visual attention task. *J. Neurosci.* **31**, 15219–15230 (2011).
49. Brainard, D. H. The Psychophysics toolbox. *Spat. Vis.* **10**, 433–436 (1997).
50. Schroeder, C. A spatiotemporal profile of visual system activation revealed by current source density analysis in the awake macaque. *Cereb. Cortex* **8**, 575–592 (1998).
51. Nigam, S., Pojoga, S. & Dragoi, V. Synergistic coding of visual information in columnar networks. *Neuron* **104**, 402–411 (2019).
52. Pettersen, K. H., Devor, A., Ulbert, I., Dale, A. M. & Einevoll, G. T. Current-source density estimation based on inversion of electrostatic forward solution: effects of finite extent of neuronal activity and conductivity discontinuities. *J. Neurosci. Methods* **154**, 116–133 (2006).
53. Zohary, E., Shadlen, M. N. & Newsome, W. T. Correlated neuronal discharge rate and its implications for psychophysical performance. *Nature* **370**, 140–143 (1994).
54. Kohn, A. & Smith, M. A. Stimulus dependence of neuronal correlation in primary visual cortex of the macaque. *J. Neurosci.* **25**, 3661–3673 (2005).
55. Kharas, N., Andrei, A., Debes, S. R. & Dragoi, V. Brain state limits propagation of neural signals in laminar cortical circuits. *Proc. Natl Acad. Sci. USA* **119**, e2104192119 (2022).

Acknowledgements

We are grateful to the excellent staff at the Center for Laboratory Animal Medicine and Care at UT Houston, in particular, C. Janssen, A. L. Trimble and M. Horscroft, for their invaluable veterinary insights. The study is funded by grants NSF/NIH CRCNS R01MH115557 and NIH RF1 MH130416 (to K.J.); NSF-DBI-1707400 (to K.J., A.E.A. and R.R.); NSF DMS-1654268 and USAF AFMC FA9550-21-1-0223 (to R.R.) and U01MH109146 and 1R01EY026156 (to V.D.).

Author contributions

A.R.A. contributed to conceptualization, methodology, software, formal analysis, investigation, data curation, writing—original draft preparation, visualization a complete list of contributions to the paper; A.E.A. contributed to methodology, software, formal analysis, writing—review and editing, visualization; N.K. contributed to formal analysis, investigation; R.R. contributed to funding acquisition, supervision, writing—review and editing; K.J. contributed to conceptualization, funding acquisition, supervision, writing—review and editing; and V.D. contributed to conceptualization, funding acquisition, supervision, writing—review and editing.

Competing interests
All the authors declare no competing interests.

Additional information
Extended data is available for this paper at https://doi.org/10.1038/s41593-023-01446-w.

Supplementary information The online version contains supplementary material available at https://doi.org/10.1038/s41593-023-01446-w.

Correspondence and requests for materials should be addressed to Ariana R. Andrei or Valentin Dragoi.

Peer review information *Nature Neuroscience* thanks Sripati Arun and the other, anonymous, reviewer(s) for their contribution to the peer review of this work.

https://doi.org/10.1038/s41593-023-01446-w

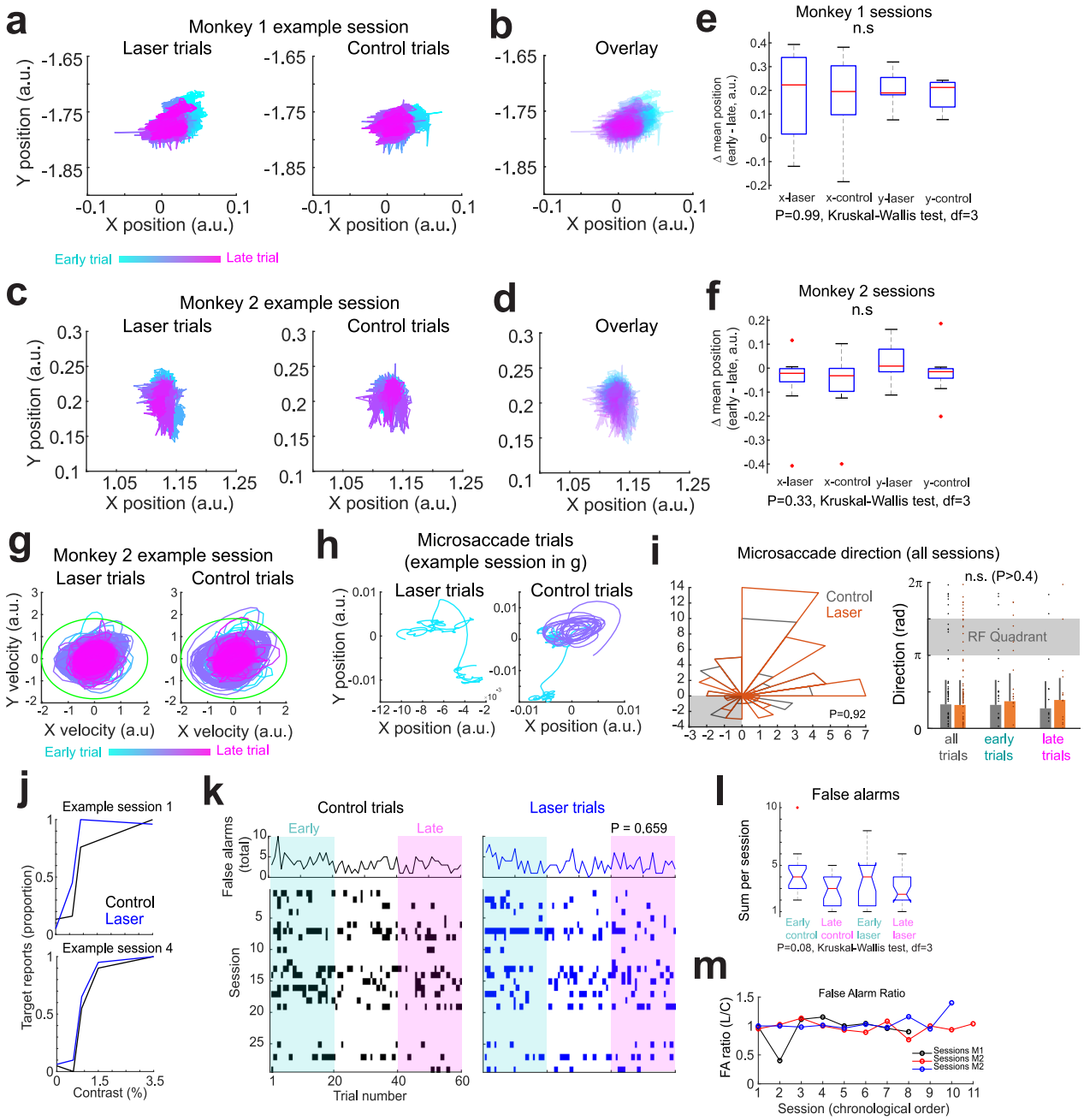

Extended Data Fig. 1 | Eye position is stable between laser and control trials across early to late trials. (a) Example eye position traces from Monkey 1. Cyan to magenta: trial order (early to late). **(b)** Superimposed laser and control traces from a. **(c–d)** Example session from Monkey 2. Same conventions as a-b. **(e)** Mean position difference between early-late trials (first, last 20 trials) for x and y coordinates across sessions from Monkey 1 (n = 7). No significant (n.s.) difference across any group. Horizontal red line: group median; edges of the box: 25th and 75th percentiles; whiskers: data extremes; red crosses: individual outliers. **(f)** Same as e, but showing sessions from Monkey 2 (n = 10). (g-i) Extensive microsaccade analysis: **(g)** Example eye velocity traces from one session. Green oval: 5 standard deviation threshold used to identify microsaccades (Hafed et al.[48]). **(h)** Eye position on trials with microsaccades from same session as in g. (i, left) Microsaccade direction circular histogram, combined for both monkeys on laser (orange) and control (gray) trials. Angle shows microsaccade direction relative to starting point; size of slice indicates the count across trials/sessions. Light gray shaded area denotes quadrant in which receptive field locations were located. No difference in mean microsaccade direction on laser versus control trials (P = 0.92, Watson-Williams test). **(i**, right) Separating cumulative microsaccade direction into early (first 20 trials) or late (last 20 trials) shows no difference between laser and control (P > 0.04 Watson-Williams test in all conditions; circular statistic). Bar graphs show mean ±s.e.m. Points show individual data points. **(j)** Two example psychometric curves from detection task. **(k)** Lower plot, false alarm raster showing trials on which false alarms were reported (first 60 trials). Upper plot shows cumulative false alarm distributions (P = 0.659, Wilcoxon ranked sum test). **(l)** Box-whisker plot of false alarms on early versus late trials (same conventions as in e-f). No difference between conditions (Kruskal-Wallis test P = 0.08; n = 29 sessions). **(m)** If monkeys were learning across sessions to ignore an optogenetically-evoked phosphene, a decreasing false alarm ratio between laser and control trials would be expected. Sessions are grouped chronologically per monkey, and separated when significant spans of time (months) separated sessions a monkey (red, blue). No temporal trends were significant for any group (Pearson correlation, P > 0.1 for all 3 session groups separately; P = 1, for all groups together).

https://doi.org/10.1038/s41593-023-01446-w

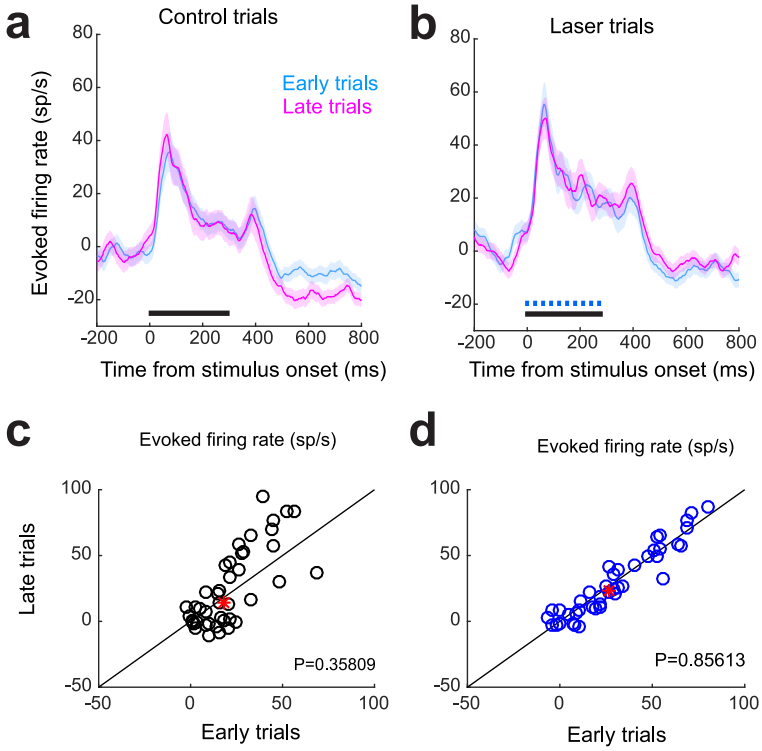

Extended Data Fig. 2 | Visual stimulus evoked responses were not different between early and late trial blocks. (a–b) Population averaged evoked stimulus response for a subset of sessions that included visual stimuli of 50% contrast (n = 42 units) for control **(a)** and laser **(b)** trials on early (blue) and late (magenta) trial blocks. Early and late trial blocks consisted of the first and last 7 trials, respectively, with no overlap. Black horizontal line shows 300 ms visual stimulus duration. Dashed blue line in b shows time period of laser stimulation (35 Hz, 10 cycles, 10 ms per cycle). (c–d) Average evoked firing rate (average firing rate during first 200 ms minus the baseline firing rate, taken 200 ms prior to stimulus onset) on early versus late trial blocks for each unit on control **(c)** and laser **(d)** trials. Red asterisk shows median. P–value result from two-sided Wilcoxon signed rank test comparing firing rates on early versus late trials for each unit.

https://doi.org/10.1038/s41593-023-01446-w

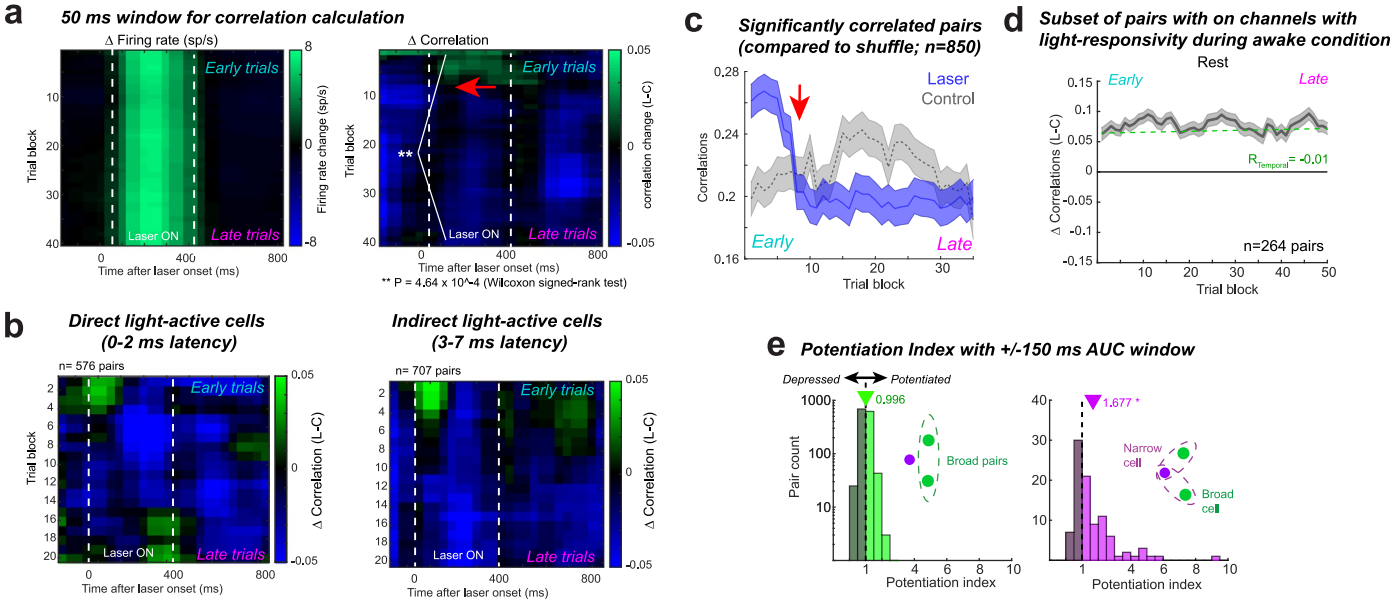

Extended Data Fig. 3 | Correlation and potentiation index results are robust to changes in time windows and cell populations used for calculations. (a) Recalculating noise correlations using a shorter 50 ms window, rather than a 200 ms window used in Fig. 1, showed a similar pattern of dynamic correlation reversal over trial blocks (indicated by the red arrow). Early versus late correlations on laser trials were significantly different from each other (** P = 0.001). Dashed vertical lines show time of laser onset and offset. **(b)** Correlation dynamics were similar if we separately considered pairs directly activated by the light (left-side panel), or indirectly via network connections (right-side panel). **(c)** We found similar effects when subselecting only significantly correlated pairs. To identify significantly correlated pairs, we shuffled control trials, and calculated correlations 1000 times. This created a distribution of chance level correlations. We next found pairs that had correlations on the first control trial block that were absolutely higher than the shuffled correlations > 95% of the chance correlations. The time- course of correlations on laser (blue) and control (gray) for these pairs is similar to the whole population of pairs (Fig. 1g). **(d)** Time course of correlation difference during rest looking only at the subset of light-responsive pairs on channels also identified as light-responsive during the awake condition (n = 264). **(e)** Recalculating the potentiation index using a larger 150 ms window around the CCG peak (rather than the 15 ms window used in Fig. 4) resulted in a similar significant increase (right-ward shift) in potentiation index distribution for narrow and broad cell pairs (purple, right side plot). This longer time window resulted in greater potentiation indices compared to the shorter time window (PI distribution means 1.68 versus 1.14, for long and short windows, respectively). Putative excitatory pairs (green, left side plot) did not exhibit a shift in the potentiation index using this longer time window (P = 0.056 Wilcoxon signed rank test). The distributions were significantly different from each other (P = 2.94E10-4, Wilcoxon ranked sum test, I-E vs. E-E, n = 1476 pairs). Arrowheads above distributions show the means. These results suggest that excitatory-excitatory and inhibitory-excitatory interactions can occur on different timescales.

https://doi.org/10.1038/s41593-023-01446-w

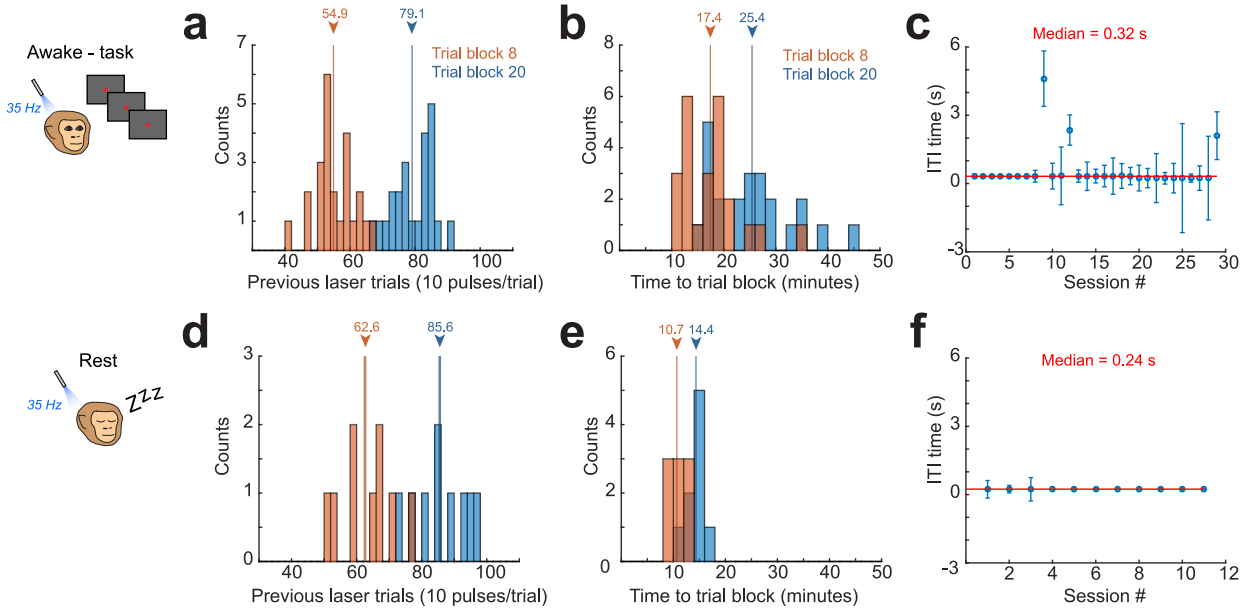

Extended Data Fig. 4 | Timing of trial events during dynamic reversal transition period. (a) Number of laser stimulation trials (all conditions) preceding trial block 8 (orange) and trial block 20 (blue) across all awake sessions (n = 29). Each laser trial consisted of 10 pulses (10 ms per pulse) at 35 Hz. Vertical lines and arrow heads show medians of each distribution. **(b)** Absolute time, in minutes, measured from the start of the first trial in a session to reach trial block 8 (orange) and trial block 20 (blue). Vertical lines and arrow heads show medians. **(c)** Distributions of inter-trial intervals for each session, measured as the end of one completed trial to the start of the next complete trial. Blue circles show session median ±s.e.m. Red horizontal line show median across all sessions. **(d–f)** Same as a-c, but for rest sessions (n = 10).

https://doi.org/10.1038/s41593-023-01446-w

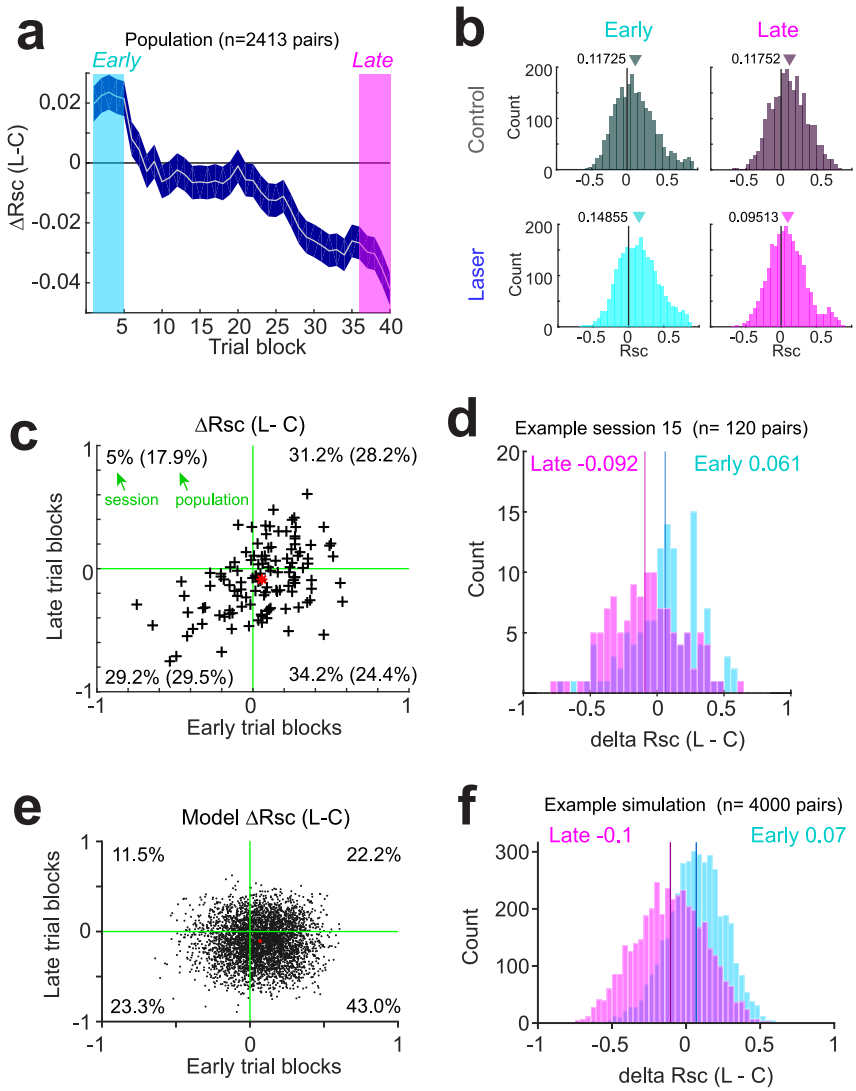

Extended Data Fig. 5 | Dynamic reversal of correlations is distributed across pairs of neurons. (a) Population correlation difference on laser versus control trials. Solid line shows mean, envelope shows s.e.m. Analysis presented in this figure compares the correlation difference on early (vertical cyan) versus late (vertical magenta) trial blocks, averaged over the first/last 5 trial blocks. **(b)** Population distributions of spike count correlations during control (top row) and laser (bottom row) conditions on early (left column) and late (right column) trial blocks. Early versus late distributions were significantly different on laser but not control trials ($P = 7.279^{-10}$, Kruskal–Wallis test, d.f. = 3, post–hoc Tukey test). Early laser distribution was significantly different from all other distributions, while the late laser distribution was significantly different from the late control distribution. **(c)** Example session data showing differences in correlations for individual pairs (n = 120). Red asterisks shows median of pairs in this session. Lower right quadrant shows pairs that exhibit both the early increase and the late decrease in correlations on laser versus control trials. Percentages denote the percent of total pairs found in each quadrant for the example session pairs (all pairs across sessions). **(d)** Distribution of early versus late noise correlation changes for the example session shown in panel c. Same conventions as panel b. **(e–f)** Same as panels c-d, but showing distributions across pairs from the model for one example simulation. Vertical lines and titles show means of early (cyan) and late (magenta) distributions.

https://doi.org/10.1038/s41593-023-01446-w

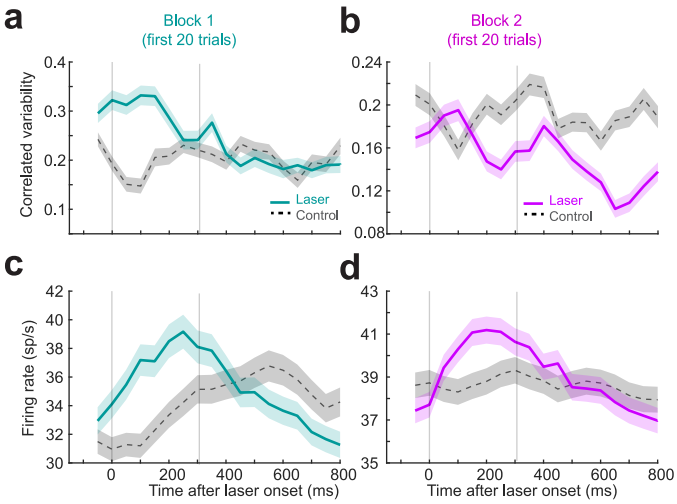

Extended Data Fig. 6 | Stimulation frequencies less than 35 Hz produce a reversal of correlation dynamics over time. (a) Correlations on laser and control trials during the first block of stimulation using only data from sessions stimulated with less than 35 Hz (unlike Fig. 2f, which also includes 35 Hz sessions; n = 243 pairs). Correlations are calculated in 200 ms windows, with a 50 ms slide. **(b)** Same as panel a, but for the first 20 trials of the second frequency block (n = 950 pairs). (**c**-**d**) Firing rates associated with laser (color, solid line) and control (gray, dashed line) trials on Block 1 and Block 2 respectively. All plots show mean and s.e.m. Vertical lines denote laser onset and offset times.

https://doi.org/10.1038/s41593-023-01446-w

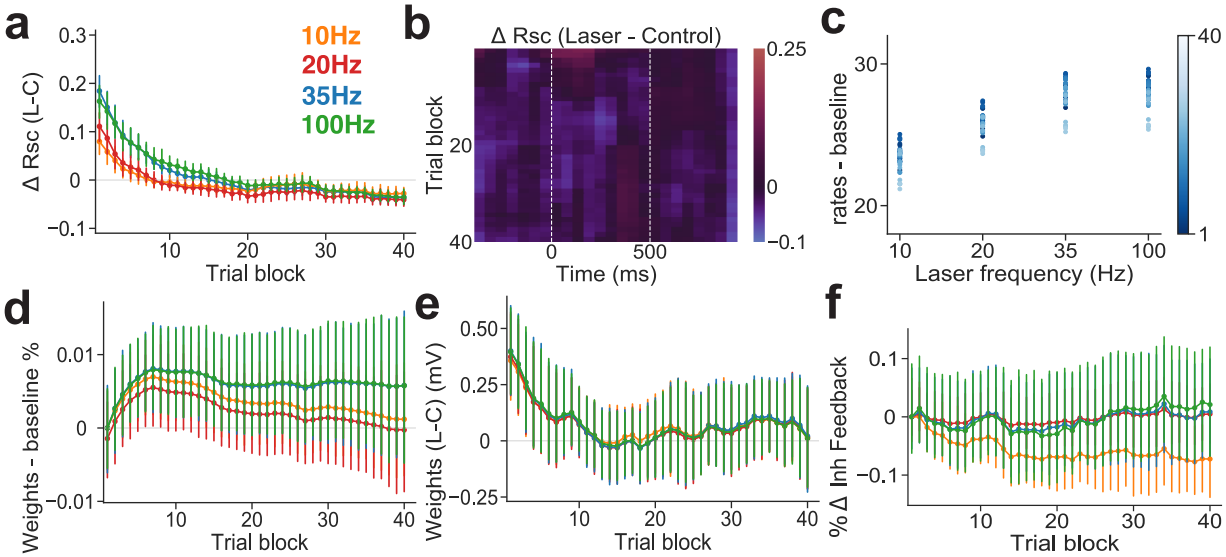

Extended Data Fig. 7 | Dynamic reversal of correlations is independent of laser stimulation frequency in network model. (a) Drop in mean correlations at center time bin of laser period for networks with varying laser stimulation frequencies. (Error shows 95% confidence intervals; n = 10 neural network simulations. Same for panels d-f). **(b)** Change in mean spike count correlations in a sample simulation of the numerical experiment in the awake condition with laser frequency 10 Hz. Correlations over the laser period drop below control due to changes in synaptic weights. **(c)** Firing rates of ChR2–expressing neurons averaged over the laser period. Higher laser frequencies evoke stronger responses. **(d)** Change in synaptic weights compared to baseline (first block) and computed over a window of 200 ms and 20 trials. **(e)** Evolution of difference in synaptic weights in laser vs control trials for different frequencies, *f*. **(f)** Mean inhibitory input to ChR2–expressing neurons changes little as changes in synaptic strengths are heterogeneous, and the network remains in balance. Inhibitory input is normalized by the first trial block, and computed over a time window of 200 ms and 20 trials.

https://doi.org/10.1038/s41593-023-01446-w

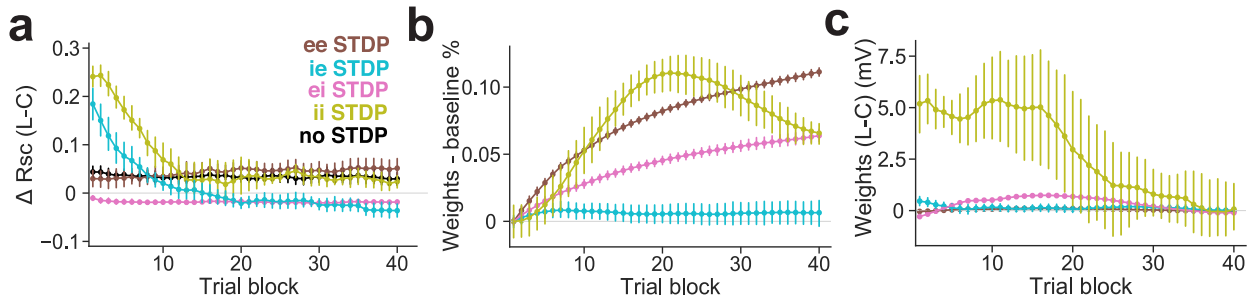

Extended Data Fig. 8 | Dynamic reversal of correlations only occurred when i-e connections were plastic in the model network. **(a)** Mean correlations at the center time bin during the laser period decreased over trial blocks when inhibitory synapses (ie or both ie and ii) were plastic. However, we observed a reversal in mean correlations, as seen in experimental data, only when ie connections were plastic, and not when both ie and ii synapses were plastic. Mean correlations remained nearly constant in the absence of STDP or when excitatory connections (ee or ei) were plastic. (Error shows 95% confidence intervals; n = 7 neural network simulations. Same for panels b-c). **(b)** Change in mean synaptic weights compared to baseline (first block) and computed over a window of 200 ms and over 20 trials. For every pair of neuronal populations where weights underwent STDP, the mean weight potentiated as a consequence of repeated stimulation and the nature of the plasticity rules. Thus, only changes in ie weights resulted in a reversal of mean correlations (panel **(a)**). **(c)** Evolution of the difference in synaptic weights in laser vs control trial blocks for different STDP rules. Under all rules, mean weights tended towards a steady state where they were approximately equal in laser and control trial blocks. However, mean weights were larger in early laser trial blocks than in early control trial blocks only under inhibitory plasticity. Thus, even though mean weights were potentiated under each STDP rule (panel **(b)**), mean correlations decreased (panel **(a)**) only when the difference between mean weights in laser vs control trials also decreased over trial blocks.

https://doi.org/10.1038/s41593-023-01446-w

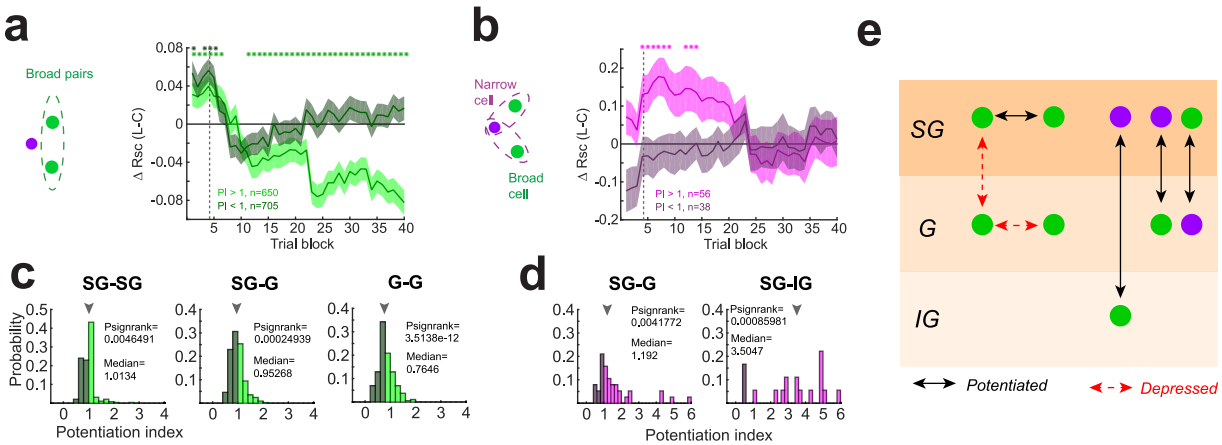

Extended Data Fig. 9 | Laminar distributions of potentiated and depressed pairs. (a) Noise correlation difference (laser minus control) for pairs of units with broad waveforms with potentiation index ('PI') > 1 (potentiated, light green) or < 1 (depressed, dark green). Asterisks indicate trial blocks in which the change in correlations was significantly different from zero (Wilcoxon signed rank test, two-sided, false discovery rate corrected, $P \leq 0.0059$). Vertical dotted line shows trial block 4, where the laser induced increase in correlated variability begins to decline between broad pairs. **(b)** Same as panel A, but for pairs of narrow and broad wave- form pairs. Asterisks indicate significantly different from zero trial blocks (Wilcoxon signed rank test, two-sided, false discovery rate corrected, $P \leq 0.0068$). Vertical dotted line shows trial block 4, where correlated variability is first significantly increased between broad-narrow cell pairs with a PI > 1. The common inflection point between panels A and B (dotted vertical line at trial block 4) suggests that broad cells become more coupled with narrow cells and simultaneously less coupled with other broad cells, consistent with the idea that I–E connections are potentiated leading to the overall decrease in correlated variability across trials. **(c)** Pairs were assigned to layers (supragranular 'SG', granular 'G', and infragranular 'IG') using the current source density method (21, 23). Distributions show potentiation indices across broad wave- form pairs in each layer combination (dark green indicates PI < 1, light green indicates PI > 1). Distributions are only shown for layer combinations in which the median PI was significantly different from unity (two-sided Wilcoxon signed rank test, P values as shown). **(d)** Same as panel c, but for narrow–broad waveform pairs. **(e)** Summary of results in panels c–d. Broad–narrow cell pairs were potentiated across SG–G and SG–IG, while broad pairs were potentiated within SG but depressed between SG–G and within G.

https://doi.org/10.1038/s41593-023-01446-w

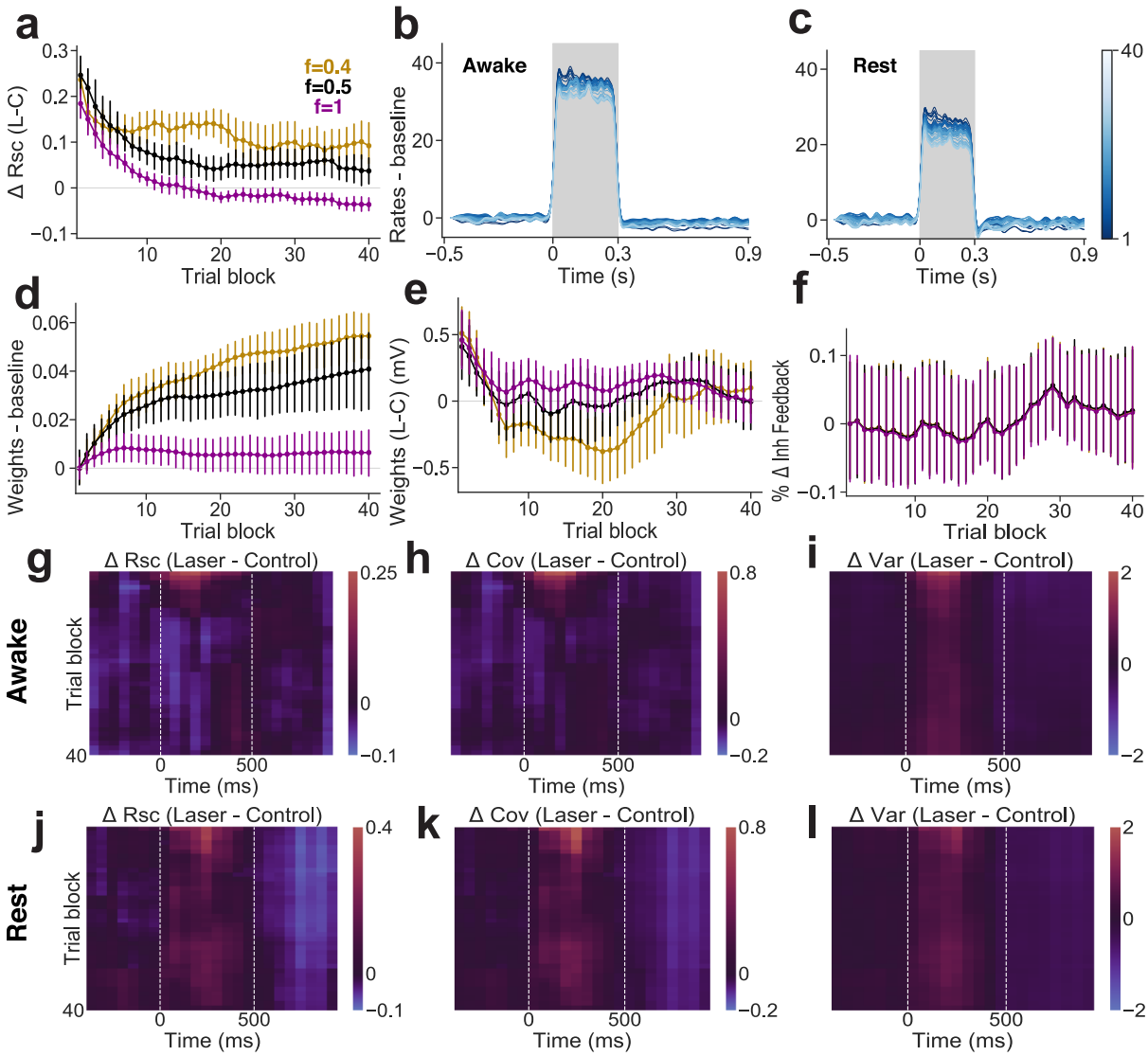

Extended Data Fig. 10 | Transition of network model from awake to rest condition. **(a)** Drop in mean correlations at center time bin of laser period for networks with varying synaptic weight scaling factors. (Error shows 95% confidence intervals; n = 10 neural network simulations. Same for panels d-f). **(b)** Peri–stimulus time histogram (PSTH) of stimulated cells in awake condition. **(c)** PSTH of stimulated cells in rest condition. **(d)** Change in synaptic weights compared to baseline (first block) and computed over a window of 200 ms and 20 trials. **(e)** Evolution of difference in synaptic weights in laser vs control trials for different values of scaling factor f. **(f)** Mean inhibitory input to ChR2–expressing neurons changes little as changes in synaptic strengths are heterogeneous, and the network remains in balance. Inhibitory input is normalized by the first trial block, and computed over a time window of 200 ms and 20 trials. **(g)** Change in mean spike count correlations in a sample simulation of the numerical experiment in the awake condition. Correlations over the laser period drop below control due to changes in synaptic weights. **(h–i)** Same as **(g)**, but for spike count covariances and variances. Changes in correlations are due to changes in covariability, not in variance. **(j–l)** Same as **(g–i)** but for 15 the rest condition (f = 0.4). Correlations, covariance, and variance remain high throughout the laser period.

nature portfolio

Corresponding author(s): Valentin Dragoi
Ariana R Andrei

Last updated by author(s): Aug. 18, 2023

Reporting Summary

Nature Portfolio wishes to improve the reproducibility of the work that we publish. This form provides structure for consistency and transparency in reporting. For further information on Nature Portfolio policies, see our Editorial Policies and the Editorial Policy Checklist.

Statistics

For all statistical analyses, confirm that the following items are present in the figure legend, table legend, main text, or Methods section.

n/a	Confirmed
☐	☒ The exact sample size (*n*) for each experimental group/condition, given as a discrete number and unit of measurement
☐	☒ A statement on whether measurements were taken from distinct samples or whether the same sample was measured repeatedly
☐	☒ The statistical test(s) used AND whether they are one- or two-sided *Only common tests should be described solely by name; describe more complex techniques in the Methods section.*
☐	☒ A description of all covariates tested
☐	☒ A description of any assumptions or corrections, such as tests of normality and adjustment for multiple comparisons
☐	☒ A full description of the statistical parameters including central tendency (e.g. means) or other basic estimates (e.g. regression coefficient) AND variation (e.g. standard deviation) or associated estimates of uncertainty (e.g. confidence intervals)
☐	☒ For null hypothesis testing, the test statistic (e.g. *F*, *t*, *r*) with confidence intervals, effect sizes, degrees of freedom and *P* value noted *Give P values as exact values whenever suitable.*
☒	☐ For Bayesian analysis, information on the choice of priors and Markov chain Monte Carlo settings
☒	☐ For hierarchical and complex designs, identification of the appropriate level for tests and full reporting of outcomes
☐	☒ Estimates of effect sizes (e.g. Cohen's *d*, Pearson's *r*), indicating how they were calculated

Our web collection on statistics for biologists contains articles on many of the points above.

Software and code

Policy information about availability of computer code

Data collection	Plexon Online Sort Client
Data analysis	MATLAB (2016a, 2019a), Microsoft Excel

For manuscripts utilizing custom algorithms or software that are central to the research but not yet described in published literature, software must be made available to editors and reviewers. We strongly encourage code deposition in a community repository (e.g. GitHub). See the Nature Portfolio guidelines for submitting code & software for further information.

Data

Policy information about availability of data

All manuscripts must include a data availability statement. This statement should provide the following information, where applicable:

- Accession codes, unique identifiers, or web links for publicly available datasets
- A description of any restrictions on data availability
- For clinical datasets or third party data, please ensure that the statement adheres to our policy

All source data used to generate experimental Figures is available at https://zenodo.org/record/7527435.

Human research participants

Policy information about studies involving human research participants and Sex and Gender in Research.

Reporting on sex and gender	N/A
Population characteristics	N/A
Recruitment	N/A
Ethics oversight	N/A

Note that full information on the approval of the study protocol must also be provided in the manuscript.

Field-specific reporting

Please select the one below that is the best fit for your research. If you are not sure, read the appropriate sections before making your selection.

☒ Life sciences ☐ Behavioural & social sciences ☐ Ecological, evolutionary & environmental sciences

For a reference copy of the document with all sections, see nature.com/documents/nr-reporting-summary-flat.pdf

Life sciences study design

All studies must disclose on these points even when the disclosure is negative.

Sample size	N=2 monkeys, similar to those reported in previous publications using similar experimental procedures
Data exclusions	Sessions were excluded if no light-responsive neurons were recorded, or if animals failed to perform the detection task (<65% correct performance on control trials using 0% or high contrast visual stimuli).
Replication	Results were replicated across animals (n=2) and sessions (n=29 sessions).
Randomization	All conditions were randomized within each session.
Blinding	Investigators were not blinded to experimental groups due to the nature of the experiments. However, all conditions were randomized in each experimental session – all conditions were present in both animals – and data was grouped automatically in MATLAB, without investigator intervention.

Behavioural & social sciences study design

All studies must disclose on these points even when the disclosure is negative.

Study description	*Briefly describe the study type including whether data are quantitative, qualitative, or mixed-methods (e.g. qualitative cross-sectional, quantitative experimental, mixed-methods case study).*
Research sample	*State the research sample (e.g. Harvard university undergraduates, villagers in rural India) and provide relevant demographic information (e.g. age, sex) and indicate whether the sample is representative. Provide a rationale for the study sample chosen. For studies involving existing datasets, please describe the dataset and source.*
Sampling strategy	*Describe the sampling procedure (e.g. random, snowball, stratified, convenience). Describe the statistical methods that were used to predetermine sample size OR if no sample-size calculation was performed, describe how sample sizes were chosen and provide a rationale for why these sample sizes are sufficient. For qualitative data, please indicate whether data saturation was considered, and what criteria were used to decide that no further sampling was needed.*
Data collection	*Provide details about the data collection procedure, including the instruments or devices used to record the data (e.g. pen and paper, computer, eye tracker, video or audio equipment) whether anyone was present besides the participant(s) and the researcher, and whether the researcher was blind to experimental condition and/or the study hypothesis during data collection.*
Timing	*Indicate the start and stop dates of data collection. If there is a gap between collection periods, state the dates for each sample cohort.*
Data exclusions	*If no data were excluded from the analyses, state so OR if data were excluded, provide the exact number of exclusions and the rationale behind them, indicating whether exclusion criteria were pre-established.*

Non-participation	*State how many participants dropped out/declined participation and the reason(s) given OR provide response rate OR state that no participants dropped out/declined participation.*
Randomization	*If participants were not allocated into experimental groups, state so OR describe how participants were allocated to groups, and if allocation was not random, describe how covariates were controlled.*

Ecological, evolutionary & environmental sciences study design

All studies must disclose on these points even when the disclosure is negative.

Study description	*Briefly describe the study. For quantitative data include treatment factors and interactions, design structure (e.g. factorial, nested, hierarchical), nature and number of experimental units and replicates.*
Research sample	*Describe the research sample (e.g. a group of tagged Passer domesticus, all Stenocereus thurberi within Organ Pipe Cactus National Monument), and provide a rationale for the sample choice. When relevant, describe the organism taxa, source, sex, age range and any manipulations. State what population the sample is meant to represent when applicable. For studies involving existing datasets, describe the data and its source.*
Sampling strategy	*Note the sampling procedure. Describe the statistical methods that were used to predetermine sample size OR if no sample-size calculation was performed, describe how sample sizes were chosen and provide a rationale for why these sample sizes are sufficient.*
Data collection	*Describe the data collection procedure, including who recorded the data and how.*
Timing and spatial scale	*Indicate the start and stop dates of data collection, noting the frequency and periodicity of sampling and providing a rationale for these choices. If there is a gap between collection periods, state the dates for each sample cohort. Specify the spatial scale from which the data are taken*
Data exclusions	*If no data were excluded from the analyses, state so OR if data were excluded, describe the exclusions and the rationale behind them, indicating whether exclusion criteria were pre-established.*
Reproducibility	*Describe the measures taken to verify the reproducibility of experimental findings. For each experiment, note whether any attempts to repeat the experiment failed OR state that all attempts to repeat the experiment were successful.*
Randomization	*Describe how samples/organisms/participants were allocated into groups. If allocation was not random, describe how covariates were controlled. If this is not relevant to your study, explain why.*
Blinding	*Describe the extent of blinding used during data acquisition and analysis. If blinding was not possible, describe why OR explain why blinding was not relevant to your study.*

Did the study involve field work? ☐ Yes ☐ No

Field work, collection and transport

Field conditions	*Describe the study conditions for field work, providing relevant parameters (e.g. temperature, rainfall).*
Location	*State the location of the sampling or experiment, providing relevant parameters (e.g. latitude and longitude, elevation, water depth).*
Access & import/export	*Describe the efforts you have made to access habitats and to collect and import/export your samples in a responsible manner and in compliance with local, national and international laws, noting any permits that were obtained (give the name of the issuing authority, the date of issue, and any identifying information).*
Disturbance	*Describe any disturbance caused by the study and how it was minimized.*

Reporting for specific materials, systems and methods

We require information from authors about some types of materials, experimental systems and methods used in many studies. Here, indicate whether each material, system or method listed is relevant to your study. If you are not sure if a list item applies to your research, read the appropriate section before selecting a response.

Materials & experimental systems

n/a	Involved in the study
☒	☐ Antibodies
☒	☐ Eukaryotic cell lines
☒	☐ Palaeontology and archaeology
☐	☒ Animals and other organisms
☒	☐ Clinical data
☒	☐ Dual use research of concern

Methods

n/a	Involved in the study
☒	☐ ChIP-seq
☒	☐ Flow cytometry
☒	☐ MRI-based neuroimaging

Antibodies

Antibodies used — *Describe all antibodies used in the study; as applicable, provide supplier name, catalog number, clone name, and lot number.*

Validation — *Describe the validation of each primary antibody for the species and application, noting any validation statements on the manufacturer's website, relevant citations, antibody profiles in online databases, or data provided in the manuscript.*

Eukaryotic cell lines

Policy information about cell lines and Sex and Gender in Research

Cell line source(s) — *State the source of each cell line used and the sex of all primary cell lines and cells derived from human participants or vertebrate models.*

Authentication — *Describe the authentication procedures for each cell line used OR declare that none of the cell lines used were authenticated.*

Mycoplasma contamination — *Confirm that all cell lines tested negative for mycoplasma contamination OR describe the results of the testing for mycoplasma contamination OR declare that the cell lines were not tested for mycoplasma contamination.*

Commonly misidentified lines (See ICLAC register) — *Name any commonly misidentified cell lines used in the study and provide a rationale for their use.*

Palaeontology and Archaeology

Specimen provenance — *Provide provenance information for specimens and describe permits that were obtained for the work (including the name of the issuing authority, the date of issue, and any identifying information). Permits should encompass collection and, where applicable, export.*

Specimen deposition — *Indicate where the specimens have been deposited to permit free access by other researchers.*

Dating methods — *If new dates are provided, describe how they were obtained (e.g. collection, storage, sample pretreatment and measurement), where they were obtained (i.e. lab name), the calibration program and the protocol for quality assurance OR state that no new dates are provided.*

☐ Tick this box to confirm that the raw and calibrated dates are available in the paper or in Supplementary Information.

Ethics oversight — *Identify the organization(s) that approved or provided guidance on the study protocol, OR state that no ethical approval or guidance was required and explain why not.*

Note that full information on the approval of the study protocol must also be provided in the manuscript.

Animals and other research organisms

Policy information about studies involving animals; ARRIVE guidelines recommended for reporting animal research, and Sex and Gender in Research

Laboratory animals — Macaca mulatta, ages 16 and 22 years

Wild animals — The study did not involve wild animals

Reporting on sex — Two males were used for this study. There is no evidence for sex-based differences in primate primary visual cortex.

Field-collected samples — the study did not involve samples collected from the field

Ethics oversight — The Animal Welfare Committee (AWC) and the Institutional Animal Care and Use Committee (IACUC) for McGovern Medical School at The University of Texas Health Science Center at Houston.

Note that full information on the approval of the study protocol must also be provided in the manuscript.

Clinical data

Policy information about clinical studies

All manuscripts should comply with the ICMJE guidelines for publication of clinical research and a completed CONSORT checklist must be included with all submissions.

Clinical trial registration	*Provide the trial registration number from ClinicalTrials.gov or an equivalent agency.*
Study protocol	*Note where the full trial protocol can be accessed OR if not available, explain why.*
Data collection	*Describe the settings and locales of data collection, noting the time periods of recruitment and data collection.*
Outcomes	*Describe how you pre-defined primary and secondary outcome measures and how you assessed these measures.*

Dual use research of concern

Policy information about dual use research of concern

Hazards

Could the accidental, deliberate or reckless misuse of agents or technologies generated in the work, or the application of information presented in the manuscript, pose a threat to:

No	Yes	
☒	☐	Public health
☒	☐	National security
☒	☐	Crops and/or livestock
☒	☐	Ecosystems
☒	☐	Any other significant area

Experiments of concern

Does the work involve any of these experiments of concern:

No	Yes	
☒	☐	Demonstrate how to render a vaccine ineffective
☒	☐	Confer resistance to therapeutically useful antibiotics or antiviral agents
☒	☐	Enhance the virulence of a pathogen or render a nonpathogen virulent
☒	☐	Increase transmissibility of a pathogen
☒	☐	Alter the host range of a pathogen
☒	☐	Enable evasion of diagnostic/detection modalities
☒	☐	Enable the weaponization of a biological agent or toxin
☒	☐	Any other potentially harmful combination of experiments and agents

ChIP-seq

Data deposition

☐ Confirm that both raw and final processed data have been deposited in a public database such as GEO.

☐ Confirm that you have deposited or provided access to graph files (e.g. BED files) for the called peaks.

Data access links *May remain private before publication.*	*For "Initial submission" or "Revised version" documents, provide reviewer access links. For your "Final submission" document, provide a link to the deposited data.*
Files in database submission	*Provide a list of all files available in the database submission.*
Genome browser session (e.g. UCSC)	*Provide a link to an anonymized genome browser session for "Initial submission" and "Revised version" documents only, to enable peer review. Write "no longer applicable" for "Final submission" documents.*

Methodology

Replicates	*Describe the experimental replicates, specifying number, type and replicate agreement.*

Sequencing depth	*Describe the sequencing depth for each experiment, providing the total number of reads, uniquely mapped reads, length of reads and whether they were paired- or single-end.*
Antibodies	*Describe the antibodies used for the ChIP-seq experiments; as applicable, provide supplier name, catalog number, clone name, and lot number.*
Peak calling parameters	*Specify the command line program and parameters used for read mapping and peak calling, including the ChIP, control and index files used.*
Data quality	*Describe the methods used to ensure data quality in full detail, including how many peaks are at FDR 5% and above 5-fold enrichment.*
Software	*Describe the software used to collect and analyze the ChIP-seq data. For custom code that has been deposited into a community repository, provide accession details.*

Flow Cytometry

Plots

Confirm that:

☐ The axis labels state the marker and fluorochrome used (e.g. CD4-FITC).

☐ The axis scales are clearly visible. Include numbers along axes only for bottom left plot of group (a 'group' is an analysis of identical markers).

☐ All plots are contour plots with outliers or pseudocolor plots.

☐ A numerical value for number of cells or percentage (with statistics) is provided.

Methodology

Sample preparation	*Describe the sample preparation, detailing the biological source of the cells and any tissue processing steps used.*
Instrument	*Identify the instrument used for data collection, specifying make and model number.*
Software	*Describe the software used to collect and analyze the flow cytometry data. For custom code that has been deposited into a community repository, provide accession details.*
Cell population abundance	*Describe the abundance of the relevant cell populations within post-sort fractions, providing details on the purity of the samples and how it was determined.*
Gating strategy	*Describe the gating strategy used for all relevant experiments, specifying the preliminary FSC/SSC gates of the starting cell population, indicating where boundaries between "positive" and "negative" staining cell populations are defined.*

☐ Tick this box to confirm that a figure exemplifying the gating strategy is provided in the Supplementary Information.

Magnetic resonance imaging

Experimental design

Design type	*Indicate task or resting state; event-related or block design.*
Design specifications	*Specify the number of blocks, trials or experimental units per session and/or subject, and specify the length of each trial or block (if trials are blocked) and interval between trials.*
Behavioral performance measures	*State number and/or type of variables recorded (e.g. correct button press, response time) and what statistics were used to establish that the subjects were performing the task as expected (e.g. mean, range, and/or standard deviation across subjects).*

Acquisition

Imaging type(s)	*Specify: functional, structural, diffusion, perfusion.*
Field strength	*Specify in Tesla*
Sequence & imaging parameters	*Specify the pulse sequence type (gradient echo, spin echo, etc.), imaging type (EPI, spiral, etc.), field of view, matrix size, slice thickness, orientation and TE/TR/flip angle.*
Area of acquisition	*State whether a whole brain scan was used OR define the area of acquisition, describing how the region was determined.*

Diffusion MRI ☐ Used ☐ Not used

Preprocessing

Preprocessing software — *Provide detail on software version and revision number and on specific parameters (model/functions, brain extraction, segmentation, smoothing kernel size, etc.).*

Normalization — *If data were normalized/standardized, describe the approach(es): specify linear or non-linear and define image types used for transformation OR indicate that data were not normalized and explain rationale for lack of normalization.*

Normalization template — *Describe the template used for normalization/transformation, specifying subject space or group standardized space (e.g. original Talairach, MNI305, ICBM152) OR indicate that the data were not normalized.*

Noise and artifact removal — *Describe your procedure(s) for artifact and structured noise removal, specifying motion parameters, tissue signals and physiological signals (heart rate, respiration).*

Volume censoring — *Define your software and/or method and criteria for volume censoring, and state the extent of such censoring.*

Statistical modeling & inference

Model type and settings — *Specify type (mass univariate, multivariate, RSA, predictive, etc.) and describe essential details of the model at the first and second levels (e.g. fixed, random or mixed effects; drift or auto-correlation).*

Effect(s) tested — *Define precise effect in terms of the task or stimulus conditions instead of psychological concepts and indicate whether ANOVA or factorial designs were used.*

Specify type of analysis: ☐ Whole brain ☐ ROI-based ☐ Both

Statistic type for inference (See Eklund et al. 2016) — *Specify voxel-wise or cluster-wise and report all relevant parameters for cluster-wise methods.*

Correction — *Describe the type of correction and how it is obtained for multiple comparisons (e.g. FWE, FDR, permutation or Monte Carlo).*

Models & analysis

n/a	Involved in the study
☐	☐ Functional and/or effective connectivity
☐	☐ Graph analysis
☐	☐ Multivariate modeling or predictive analysis

Functional and/or effective connectivity — *Report the measures of dependence used and the model details (e.g. Pearson correlation, partial correlation, mutual information).*

Graph analysis — *Report the dependent variable and connectivity measure, specifying weighted graph or binarized graph, subject- or group-level, and the global and/or node summaries used (e.g. clustering coefficient, efficiency, etc.).*

Multivariate modeling and predictive analysis — *Specify independent variables, features extraction and dimension reduction, model, training and evaluation metrics.*